

Control of the produced water scaling potential: an example from the Halfdan field (North Sea)

Master Thesis in Oil and Gas Technology

Erica Dos Santos Godinho

7TH JUNE 2018

Supervisor:
Professor Erik Gydesen Søgaard



Department of Chemistry and Bioscience
Aalborg University Esbjerg

Title Page

Project from: Aalborg University Esbjerg (AAUE)

Address: Niels Bohrs Vej 8, 6700 Esbjerg, Denmark

Study: Oil and Gas Technology, Master Degree

Semester: 10th Semester

Code: K10-OG3-F18

Project title: Control of the produced water scaling potential: an example from the Halfdan field (North Sea)

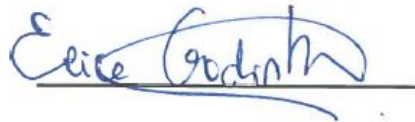
Author: Erica dos Santos Godinho

Supervisor: Professor Erik Gydesen Søggaard

Project period: February – June 2018

Submission date: 7th June 2018

By signing the author take the full responsibility for the contents of the master thesis.



(Erica dos Santos Godinho)

Acknowledgements

The author would like to express her gratitude to Erik G.Søgaard for the support, technical advice and encouragement provided throughout the entire process.

The author would like to thank Total, S.A. (Maersk olie og gas) for providing the offshore samples, and for the opportunity to write this thesis; without the samples the "real" value of this project would not be the same.

A word of appreciation is also more than deserved for the laboratory technicians. Dorte and Linda thank you for being always available to share your knowledge, for providing guidance and for helping me to built the confidence to operate all equipments and to do the analysis myself. Lisbet thank you for the support and explanations.

A special word for Mette, the secretary of studies for the chemistry and biochemistry department, for being supportive, efficient and helpful, whenever some bureaucratic problems would come to light. Your kind words were always an inspiration.

I would like to thank my colleagues and friends Frida, Konstantinos and also Nikos for the great time we had together in the lab. Working long hours turns to be easy when you have such a happy environment. Mathias, my danish friend, thank you a lot for all the help with the GCFID and discussions about the results, your inputs were always of great help. Konstantin and Paulius, the "office" guys, thanks for all the fun moments, the laughs and encouragement words, finally we are O&G engineers :). Jaqueline (Jaq) thank you for you kindness and patience to teach me to operate the core flooding equipment and for all the support through out the project.

A special gratitude to Marta "Maria", my friend of all times :), thank you, essentially for being my friend, for proof-reading my thesis and the extended abstracts for the conferences, for sharing your opinion regarding my work, for your support and comforting words when there were most needed. Ricardo thank you for all the fun and great moments, they helped a lot to get my brain rested.

At last, my words are not enough to express my gratitude towards my husband Murphy and my parents. Murphy thank you for always being there at the right moment to support me, for making me feel safe and for understanding all the times I couldn't give you as much attention as you deserve! "Papás" thank you a lot for showing the confidence you have in me, for teaching me to be strong and for always encouraging me to do my best.

To the memory of my grandmother "Avó Josefina", I know you were always with me, helping me from there, encouraging me to fight for my dreams to come true. You are and you will always be in my mind!

Abstract

Scale formation has been considered a major problem in the oil and gas industry. The mineral precipitation can pose a serious threat to oil and gas production both at a surface (production facilities) and subsurface (reservoir and near- wellbore region) level.

The scale deposition can result in a decreased production and end up in well loss. The current research investigated the scale potential associated to the an offshore produced water sample (Halfdan field - North Sea) if exposed to two different formation waters (Ekofisk and Valhall) at 70°C.

The coreflooding experiments at constant flow-rate have demonstrated the occurrence of porosity reduction (ca. 1.3% in one of the cases) and permeability decrease, approximately 0.017 D in both cases. Moreover, the experimental results have indicated the possibility of barite precipitation, tendency for potassium, carbonate and bicarbonate ions retention and localized phosphate dissolution.

Resumo

A formação de incrustação inorgânica tem vindo a ser considerada um problema de extrema importância na indústria petrolífera. A precipitação mineral pode representar uma séria ameaça para a produção de hidrocarbonetos, nomeadamente ao nível de superfície (instalações de produção) ou subsuperfície (reservatório ou zona circundante do poço).

A deposição de incrustação inorgânica pode resultar num decréscimo de produção ou até mesmo causar perda de poços. Este trabalho investigou o potencial de formação de incrustação inorgânica associado a uma amostra de água produzida (do campo Halfdan - Mar do Norte) se exposta a duas águas de formação diferentes (Ekofisk e Valhall) para uma temperatura constante de 70°C.

Os resultados experimentais do "coreflooding" para um fluxo de injeção constante vieram demonstrar a ocorrência de redução de porosidade (aproximadamente 1.3% num dos casos) e decréscimo de permeabilidade em aproximadamente 0.017 D em ambos os casos. Mais ainda, os resultados experimentais indicaram a possibilidade de precipitação de barite, tendência para retenção de potássio, carbonato e bicarbonato e dissolução localizada de fosfato.

Nomenclature

Symbol	Definiton
η	Viscosity [cP]
ΔP	Variation [atm]
γ_x	activity coefficient of component x
μm	Micrometers
σ	Interfacial tension
ϕ	Porosity [%]
\sim	approximately
[x]	Concentration of component x [g/l]
BHP	Bottom hole Pressure
BN	Base number [mgKOH/g]
BPR	Back-pressure Regulator
BTX	Benzene, Toluene and Xylene
ca.	Approximately/circa
CBR	Crude oil - Brine (<i>s.l.</i>) - Rock system
cm	centimeters
dP	Voltage differential [V]
dU	Pressure differential [bar]
DCG	Danish Central Graben
DK	Denmark
DI water	Deionized water
e.g.	for example
EOR	Enhanced Oil Recovery
E&P	Exploration and Production
EFW	Ekofisk Formation Water
F	degree Fahrenheit
FW	Formation Water

Nomenclature

g	grams
GC	Gas Chromatography
GCFID	Gas Chromatography with Flame Ionization Detector
HPHT	High Pressure, High Temperature wells
IC	Inorganic carbon
ICP-OES	Inductively Coupled Plasma-Optical Emission Spectrometry
<i>i.e.</i>	that is/id est (latin)
IS	Ionic Strength [mg/l]
K	Permeability [D]
Ma	Million years
mD	millidarcy
MFT	Modified Flotation Technique
mg	milligrams
MM_{scf}	million standard cubic feet
O&G	Oil and Gas
OIW	oil in water (ppm)
OSPAR	Oslo/Paris convention
P conf.	Confining pressure [psi]
PDA	Potential Determining Anions
PDI	Potential Determining Ions
PMT	Photomultiplier tube
PSFI	Potential Scale Forming Ions
Psi	Pound per square inch, equal to lbf/in^2
PW	Produced water
QC	Quality Control
Ref.	Reference
SI	Saturation Index
Sat. weight	Saturated weight
<i>s.l.</i>	sensu latu/in a broad sense
TC	Total Carbon [g/l]
TDS	Total dissolved solids [g/l]
TOC	Total organic carbon [g/l]
TIC	Total inorganic carbon [mg/l]

Nomenclature

USA	United States of America
VFW	Valhall Formation Water
VOCs	Volatile organic compounds
WAG	Water alternating gas flooding

Table of Contents

Title Page	i
Acknowledgements	ii
Abstract	iii
Resumo	iv
Nomenclature	v
1 Problem Definition	1
2 Introduction	2
2.1 The North Sea Reservoir	2
2.1.1 North Sea chalk	4
2.2 Austin Chalk	5
2.3 The phenomenon of scaling	6
2.3.1 Scale Induction: typical scenarios	8
2.3.2 Scale types and its prediction	9
2.3.3 Scale Prevention and Treatment	15
2.4 Analytical Techniques	17
2.4.1 Inductively Coupled Plasma - Optical Emission Spectrometry (ICP– OES)	17
2.4.2 Ion Chromatography (IC)	17
2.4.3 Gas Chromatography with Flame ionization Detector (GC-FID)	18
2.4.4 Total Carbon (TC)	20
2.4.5 X-ray Fluorescence (XRF)	21
3 Experimental Work	22
3.1 Experimental Materials and Techniques	22
3.1.1 Rock samples	22
3.1.2 Formation and Produced water samples	22
3.1.3 Analytical Techniques	23
3.1.4 Beaker Test	30
3.1.5 Coreflooding Analysis	33

4	Results and Discussion	40
4.1	General Principles	40
4.1.1	Beaker Test	40
4.1.2	Coreflooding Experiments	42
4.1.3	Ionic Compositions: results from ICP-OES, IC and TC	51
4.1.4	Final Remarks	56
5	Conclusions	59
5.1	Future Work	61
	Bibliography	62
A	Appendix	66
A.1	ICP-OES Calibration Curves	66
A.2	ICP-OES Spectrum	69
A.3	Ion Chromatography Calibration Curves	70
A.4	Ion Chromatogram	73

List of Tables

2.1	Worldwide revenues by region and application in terms of Scale control chemicals. [20]	4
2.2	Oilfield most common scale minerals. [6, 33]	9
3.1	Dan Chalk and Austin Chalk chemical compositions. Results provided by XRF analysis.	23
3.2	Ekofisk Formation Water and Valhall Formation water chemical compositions.	24
3.3	Metals wavelengths (nm) analyzed in ICP-OES measurements.	25
3.4	Concentration of the standards 1,2 and 3 for ion chromatography.	26
3.5	IC Multi-Element Standard– 7 Elements: Concentration and QC [37]	27
3.6	Standard concentrations in mg/l for the total carbon analyzer.	29
3.7	Core samples data used in porosity and permeability measurements.	34
3.8	Core sample dry and saturated weight before coreflooding experiments.	37
3.9	Core sample saturated weight after coreflooding experiments and core sample dry weight (exposure to 100°C) after coreflooding experiments.	38
4.1	Porosity and permeability of the AC3 core sample of Austin Chalk before Ekofisk formation water saturation and coreflooding. Results from AP-608 automated permeameter-porosimeter.	46
4.2	Porosity and permeability of the AC3 core sample after coreflooding. Results from AP-608 automated permeameter-porosimeter.	46
4.3	Porosity and permeability of the AC4 core sample of Austin Chalk before valhall saturation and coreflooding. Results from AP-608 automated permeameter-porosimeter.	51
4.4	Ionic composition (ppm), ionic strength (mol/l), density (g/cm^3) and pH presented by Ekofisk brine (EFW), Valhall brine (VFW) and Halfdan produced water (HPW).	58

List of Figures

2.1	Geographical distribution of the oil and gas field in the North Sea. Source [13].	3
2.2	Homogeneous nucleation process chain. Source [4].	7
2.3	Heterogeneous nucleation phenomenon. Source [4].	7
2.4	Mineral scale solubilities (ppm) <i>versus</i> temperature (F). [27]	10
2.5	Carbon dioxide, bicarbonate and carbonate ions equilibrium dependence on pH for various fractions of carbonic acid in seawater. Source [4].	11
2.6	Major components and layout sketch of a typical ICP-OES. PMT stands for photomultiplier tube. Source [7].	18
2.7	Block diagram of the ion chromatography systems, in which C: Separating column; D: Detector; E: Eluent; I: Injector; M: Suppressor Module; PC: computer; PR: Printer; S: Probe; W: Waste; 818: IC pump; 819: IC detector; 820: IC Separation center and 830: IC interface. Source [18].	19
2.8	Schematic representation of the GC-FID equipment, in which 1: Gas carrier; 2: Flow controller valve; 3: Injector port; 4: Column; 5: Thermostatic oven; 6: Detector (FID); 7: Recorder and 8: Waste line for gathering of paralyzed products. Courtesy of Mathias K. Jørgensen.	20
3.1	Calibration curve for crude-oil. Courtesy of Mathias K. Jørgensen.	28
3.2	Preparation of the autoclave flask with the chalk and selected brine (<i>s.l.</i>).	32
3.3	pH measurement of the brine (<i>s.l.</i>) after 24h of exposure to the rock.	32
3.4	Pure water dynamic viscosity (cP) and density (g/cm^3) for various Temperatures. Source [34].	36
3.5	Simplified schematic representation of the coreflooding equipment.	37
3.6	Volumetric funnel and desiccator for core saturation.	38
4.1	Danchalk pH variation upon interaction with Ekofisk formation water, Valhall formation water and Halfdan produced water at temperatures of 20°C and 70°C.	41
4.2	Austin Chalk coreflooding output flow-rate.	42
4.3	Austin Chalk coreflooding effluent pH variation over time.	43
4.4	Raw data for CF2 differential pressure variation (bar) over time.	44
4.5	CF2 differential pressure variation (atm) over time used for permeability calculation.	45
4.6	Annulus Pressure variation (bar) over time during CF2 coreflooding.	45

List of Figures

4.7	Ekofisk FW saturated Austin Chalk permeability variation (D) over time upon coreflooding with HPW at constant flow-rate (1ml/min) and constant T of 70°C.	45
4.8	Permeability (D) <i>versus</i> differential pressure (atm) for Austin Chalk AC3 sample saturated with Ekofisk formation water and flooded with Halfdan produced water.	47
4.9	Raw data for CF3 differential pressure variation (atm) over time.	48
4.10	CF3 differential pressure variation (atm) over time used for permeability calculation.	49
4.11	Annulus Pressure variation (bar) over time during CF3 coreflooding.	49
4.12	Valhall FW saturated Austin Chalk AC4 sample permeability variation (D) over time upon coreflooding with HPW at constant flow-rate (1ml/min) and constant T of 70°C.	50
4.13	Permeability (D) <i>versus</i> differential pressure (atm) for Austin Chalk saturated with Valhall formation water and flooded with Halfdan produced water.	50
4.14	Cationic concentrations of Halfdan produced water (inlet), Ekofisk and Valhall formation waters normalized to seawater composition. For display purposes, Ba concentrations of 0 mg/l have been increased to 0.05 mg/l.	52
4.15	Ionic concentrations of produced water (inlet), Ekofisk and produced water effluents normalized to seawater composition. For display purposes, Ba concentrations of 0 mg/l have been increased to 0.05 mg/l.	53
4.16	Ionic concentrations of produced water (inlet), Valhall and produced water effluents normalized to seawater composition. For display purposes, Ba concentrations of 0 mg/l have been increased to 0.05 mg/l.	54
4.17	Total organic carbon content of Halfdan produced water prior to injection and in coreflooding effluents. Results acquired by Analytik jena multi N/C 2100 analyzer.	55
4.18	Total inorganic carbon content of Halfdan produced water prior to injection and in coreflooding effluents. Results acquired by Analytik jena multi N/C 2100 analyzer.	56
A.1	Ba 233.527 and Fe 238.204 calibration curves, showing the correlation coefficient close to 1.	66
A.2	K 766.490 and Mg 279.553 calibration curves, showing the correlation coefficient close to 1.	67
A.3	Na 589.592 and Zn 213.857 calibration curves, showing the correlation coefficient close to 1.	67
A.4	Sr 421.552 and Ca 317.933 calibration curves, showing the correlation coefficient close to 1.	68
A.5	Example of ICP-OES result provided for Na by Perkin Elmer Optima 8000 analyzer.	69
A.6	Chloride ion calibration curve, showing the correlation coefficient close to 1.	70
A.7	Sulfate ion calibration curve, showing the correlation coefficient close to 1.	71
A.8	Bromide ion calibration curve, showing the correlation coefficient close to 1.	72

A.9 Example of chromatogram result provided by Metrohm Ion Chromatography analyzer. 73

1 Problem Definition

Scale formation has been considered a major problem in the oil and gas industry. The precipitation and accumulation of minerals can pose a serious threat to oil and gas production both at a surface and subsurface level. The scale deposition can result in a decreased production and end up in well loss.

Flow assurance is a top priority for all operators, therefore mitigation strategies and control measures should be taken in order to prevent, control or treat scale formation.

The primary objective of this work is to investigate the scaling potential that can be associated with produced water injection in pressure maintenance and advanced waterflooding. Main focus will be placed on:

1. the understanding of the scale formation mechanisms;
2. the control of the main parameters that induce or affect mineral scale formation;
3. to test different formation water compositions, to understand how the influence scale deposition and accumulation;
4. investigate the scale formation associated with produced water injection for the Halfdan field.

2 Introduction

The production of hydrocarbons fluids is normally accompanied by water production. The ratio of produced water/hydrocarbons has a tendency to increase as the field enters a mature stage and gets depleted.

The increased environmental responsibility and consciousness have led to the search of new possibilities of usage for the produced water. The produced water discharges are subjected to very strict regulations and its treatment is normally very expensive. Besides the involved costs, if the produced water is discharged, there is a possibility of being wasting potential valuable asset. Therefore, produced water management should carefully evaluated, and its re-use shall be regard as a serious possibility. However, in order to use it, one should thoroughly investigate the potential of salt deposition (i.e., scale potential) for downhole and upstream conditions, particularly in terms of pressure, temperature, pH and presence of acidic gases.

2.1 The North Sea Reservoir

The North Sea reservoirs are essentially located in a specific type of carbonate rock, named chalk and in weakly cemented sandstone rocks. In terms of geographic location, the oil and gas fields are distributed as can be seen in Figure 2.1.

The tectonic history and failed rifting during the latest Jurassic and earliest Cretaceous are fundamental to understanding oil and gas in the North Sea (Brooks and Glennie, 1987; Pegrum and Spencer, 1990 in [13]). The geological evolution of the North Sea is characterized by the occurrence of three major events: the pre-rift, the syn and post-rift events [13]. "The Mesozoic rifting event controlled the major structural pattern overprinted by younger tectonic events, which have greatly influenced the sedimentation style. During the Late Cretaceous and Early Tertiary, a strike-slip faulting regime took place in the graben

and gave rise to the inversion tectonics. These movements and halokinesis initiated the development of the chalk structures"[31], that have been drilled. The Danish part of the North Sea is described as being in continuity with the Norwegian sector. In danish sector the generated hydrocarbons are of Upper Jurassic origin, and Palaeocene claystones provided the seal for the accumulation. In general the productive intervals consist of chalk of the Ekofisk and Tor Formations. [9]

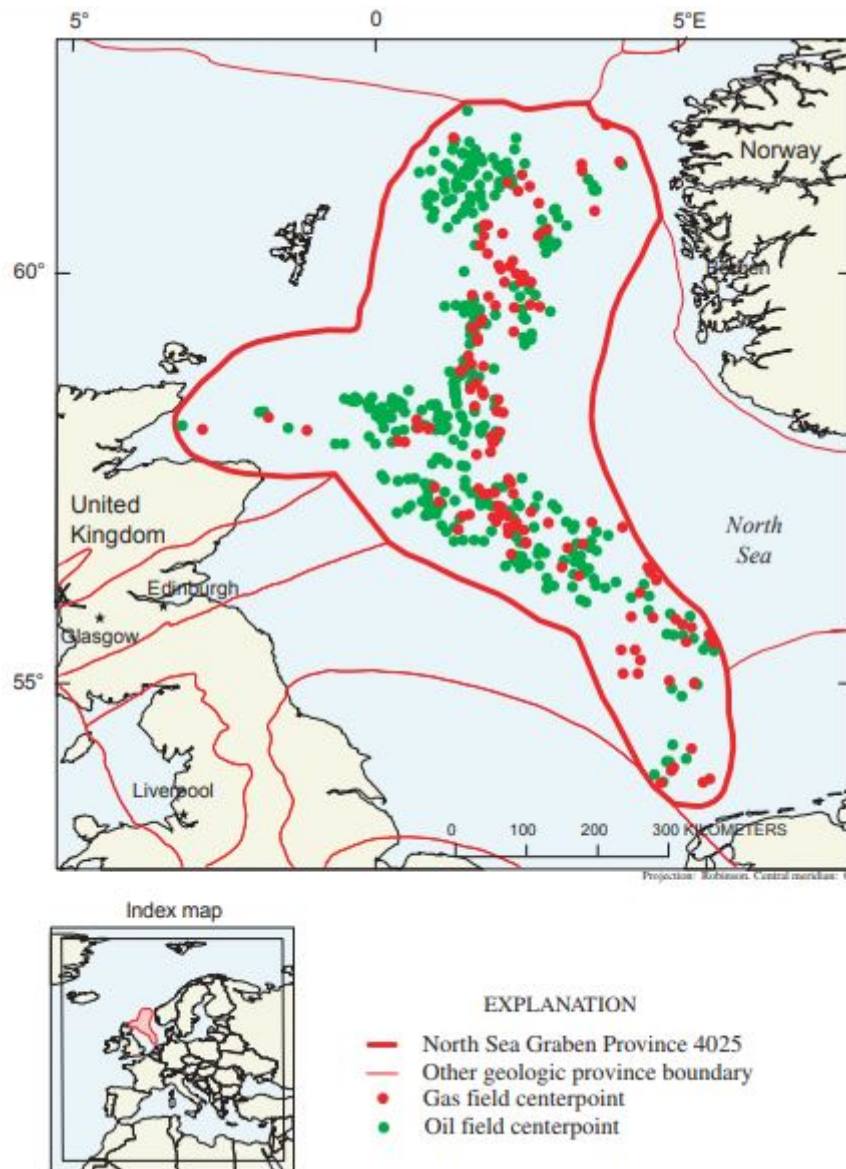


Figure 2.1: Geographical distribution of the oil and gas field in the North Sea. Source [13].

The North Sea is described as a scale prone region, therefore requiring large investments in scale treatments, see Table 2.1.

Table 2.1: Worldwide revenues by region and application in terms of Scale control chemicals. [20]

Region	Revenues (\$ million) 2002		
	Topside	Downhole	Total
North America	20	8	28
South America	5	2	7
Europe (excl N Sea)	2	1	3
North Sea	20	27	47
Russia	5	0	5
North Africa	7	3	10
West Africa	4	1	5
Middle east	6	2	8
Far East/Australasia	6	4	10
Total	76	47	123

2.1.1 North Sea chalk

The geological term chalk is used to describe a particular type of limestone, which is characterized by its whiteness, purity, friability and continuous depositional extent over several continents for half a geological period [15, 10]. Petrophysical properties of the reservoir rock might vary within the same reservoir. Therefore, the evaluation of the reservoir rock and subsequent studies must account for these oscillations. Ekofisk field (Norway) is one of the most studied fields and can serve as an example of a North Sea chalk Reservoir. In general terms, this field is characterized by high-porosity fine-grade chalk, a limestone composed of coccolith fragments. The latter correspond to skeletal debris of unicellular algae (Coccolithophorids). Complete coccoliths are found in chalks, but the majority are broken up into their minute components termed coccolith platelets or laths. Each lath is a tablet-shaped crystal of low magnesian calcite, typically = 0.5-1 μm [9]. The chalk porosity vary between 10 and 48%, depending on the geological history of each place. The relation between the porosity and permeability is not direct and even the high porosity chalk has relatively low matrix permeability (i.e., the permeability of the matrix

itself) between 1 and 5 mD. Natural fractures provide high fracture permeability (i.e., the permeability caused by the macroscopic fractures) resulting in total chalk permeability ranging from 10 to 100 mD. [21]

The chalk in the central graben area is of pelagic origin and formed from settling of calcareous nannoplankton remains (coccoliths), consisting generally of 95–99% calcite [19], which is the most stable polymorph of $CaCO_3$ for most pressures and temperatures. Aragonite and vaterite are the two other $CaCO_3$ polymorphs, which occur at particular pressure and temperature conditions [10].

Halfdan Field

The Halfdan field is located in the salt dome province of the Danish Central Graben (DCG) offshore west Denmark. The DCG consists of a complex of NNW–SSE half-grabens, and a subordinate N–S-trending segment to the south extending into the German and Dutch sectors [1]. The main bounding fault in the Danish sector is the Coffee Soil Fault, which forms the eastern margin of the Danish Central Graben (Andsbjerg & Dybkjær, 2003 in [1]). "The Central Graben is however not a simple rift graben: the faulting, folding and subsidence patterns in the region are complex and not yet fully understood (Gowers & Sæbøe, 1985). This complex architecture is due to a combination of fault re-activation, salt movements and inversion tectonics" [1].

The Halfdan reservoir is characterized by a low permeability chalk of Maastrichtian and Danian ages (Upper Cretaceous to Paleocene, around 70 Ma). The Danian and Maastrichtian formations are separated by a hard ground with extremely low permeability (Hansen & Nederveen, 2005 in [1]). At reservoir levels, the porosity ranges between 25 and 30%, with permeabilities ranging from 0.5 to 2.0 mD. The Danian chalk sample has a tendency to show 5 to 15 times lower permeability if compared to Maastrichtian formation for the same porosity chalk. [1]

2.2 Austin Chalk

The Austin Chalk is considered one of the most productive formations in South-central Texas and southern Louisiana regions (USA), that had its boom during the 1970s and early 1990s [25]. It consists of recrystallized, fossiliferous, interbedded chalks and marls

and is dated from the Upper Cretaceous (Coniacian to Campanian, about 85 Ma). "The Austin Chalk ranges in thickness from 45 to 243 meters and has many named members. In a broader and regional scale it has been classified into three main units: the lower chalk, the middle marl, and the upper chalk. The upper and lower chinks contain less clay and are therefore better reservoirs because they are more brittle, leading to higher fracture density (Hovorka and Nance, 1994)" [36]. Essentially, it consists of a large accumulation of coccoliths, which are calcium carbonate microplates that constitute the exoskeleton of the coccolithophore - a unicellular plankton (see above). "The Austin Chalk is considered a low-porosity, low-permeability carbonate. It has a matrix composed of micropores ranging in size from 5 to 7 microns and a moderately interconnected fracture system. The matrix porosity commonly ranges from 3 to 10 % and generally decreases with depth"[36]. Regarding the permeability, it also decreases with depth, and it is typically near 0.5 mD and locally around 0.1 mD (Dawson and others, 1995 in [36]), but locally can reach 1.27 mD [25]. Such low porosity and especially low permeability, imply that production must rely heavily on fracture porosity and permeability. Water saturation is generally high, from 45 to 80 %, and residual oil saturation ranges from 10 to 50 % (Dawson and others, 1995 in [36]).

2.3 The phenomenon of scaling

Scale consists in the accumulation of precipitated minerals, that turn into hard deposits sometimes coated by tar-like or waxy hydrocarbons that protects it from being dissolved with acids, for example if calcium carbonate scale is considered [8, 12]. In the literature it is also known as inorganic fouling or crystallization fouling.

The scaling phenomenon might be favored by changes in temperature, pressure, pH, mixing of incompatible waters. However, the oversaturation of produced water and its classification as scale-prone waters does not necessarily mean they will produce scale.[8] In order to develop scale there must be nucleation. The nucleation process can appear as (adapted from[8]):

1. Homogeneous nucleation (Fig.2.2): Spontaneous process in which a supersaturated solution leads to the formation clusters of ions that form single crystals. These crystals will act as seeds and grow by adsorbing ions onto imperfections. This way the crystal size increases.

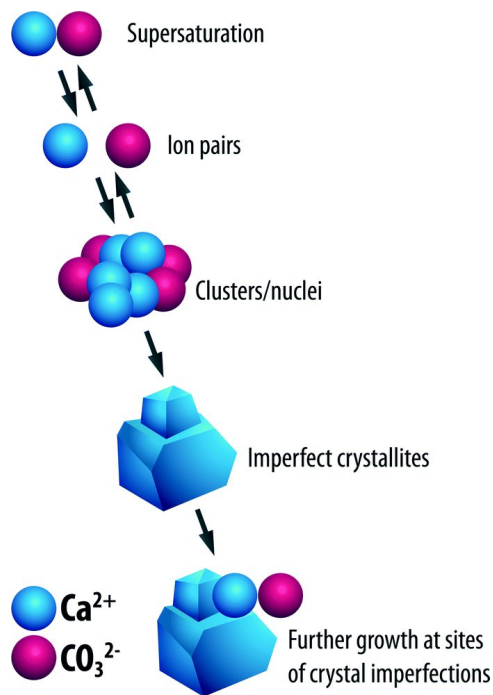


Figure 2.2: Homogeneous nucleation process chain. Source [4].

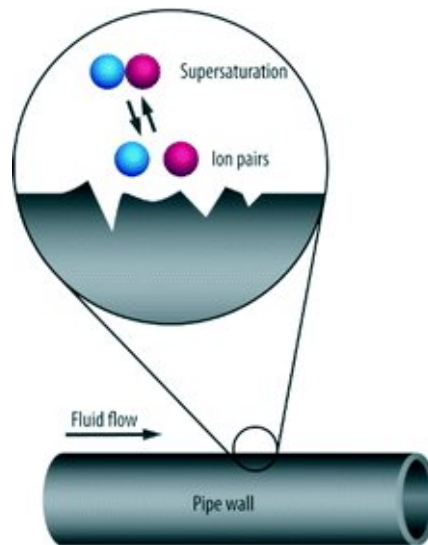


Figure 2.3: Heterogeneous nucleation phenomenon. Source [4].

2. Heterogeneous nucleation (Fig.2.3): high degree of turbulence induces the deposition of scale. The nuclei form preferentially at structural heterogeneities and are considered a "foreign" particle. The presence of imperfections in pipelines, perforations in production liners, joints and seams in tubing and pipelines provide the necessary conditions for scale formation.

2.3.1 Scale Induction: typical scenarios

The formation and precipitation of scale is frequently associated to one phenomenon or combination of the phenomena listed below [8]:

1. **Incompatible Mixing:**

Injection of seawater into the reservoir for pressure maintenance or EOR operations can lead to scale deposition. This happens due to the interaction of divalent cations largely present in formation waters with the high sulfate content that characterize seawater – frequently over 2000 ppm. If the solubility limit for any of the sulfate compounds is exceeded, scaling will occur;

2. **Self-scaling or Autoscaling:**

Direct: the pressure and temperature changes that occur as the reservoir fluid is produced might induce scaling if these changes take the fluid composition beyond the solubility limit for a certain mineral;

Indirect: a common example of indirect self-scaling occur when the reservoir fluid contains acid gases. The sudden decrease in pressure can partially release the gases, which will cause an increase in the pH, consequently inducing carbonate scale deposition. Additionally, the temperature has the reverse effect.

3. **Evaporation:**

The production of wet-gas frequently induces scale deposition. Such phenomenon occurs due to the hydrostatic pressure decrease in production tubing, which promotes volume expansion of the gas and the evaporation of the brine. High pressure, high temperature wells (HPHT) commonly have halite scale that has been formed in association with the previous process;

4. **Gas flood:**

The gas flood is a commonly used EOR method, sometimes associated with water-flooding in a process called WAG. As an example, such phenomenon, is once again connected to the fact that CO_2 will dissolve in the water, which will become acidic, being capable of dissolving the calcite in the reservoir. If a pressure drop occur, the acid gas will be liberated and the pH will rise leading to a deposition of calcite.

2.3.2 Scale types and its prediction

The scale types are in general well described and in a broad sense can be divided into sulfate and carbonate scales. Prediction of scaling potential in hydrocarbon system is normally complicated but rather important, as scale precipitation is capable of smother a productive well in 24 hours – e.g. Miller field (North Sea) [8].

The mineral scale prediction is generally made by looking into saturation indexes, which compare the quantity of scale components present in solution to the solubility. [26, 32] In general, accurate predictions will require brine pH measurements, however in oil and gas wells real pH measurements are rarely feasible.

The most common oilfield scale types are presented in Table 2.2, which also refers the primary parameter able to disturb the chemical equilibrium leading to a possible reduction in terms of solubility and therefore lead to mineral precipitation. The most common mineral scale solubilities relation with temperature can be seen in Figure 2.4.

Table 2.2: Oilfield most common scale minerals. [6, 33]

<i>Mineral Scale</i>		<i>Chemical Formula</i>	<i>Primary Influencer Parameter</i>
Calcium Carbonate		CaCO ₃	CO ₂ partial pressure, T, TDS and pH
Calcium sulfate	Gypsum	CaSO ₄ .2H ₂ O	T, TDS and P
	Hemihydrate	CaSO ₄ .H ₂ O	
	Anhydrite	CaSO ₄	
Barium sulfate		BaSO ₄	T and P
Strontium Sulfate		SrSO ₄	T, P and TDS
Iron components	Ferrous Carbonate	FeCO ₃	Corrosion, dissolved gases and pH
	Ferrous Sulfide	FeS	
	Ferrous Hydroxide	Fe(OH) ₂	
	Ferric Hydroxide	Fe(OH) ₃	

Carbonate scales

The carbonate scales is a general term used to refer to all the potential scale minerals that have in its structure the carbonate ion. The mineral scales belonging to this group are:

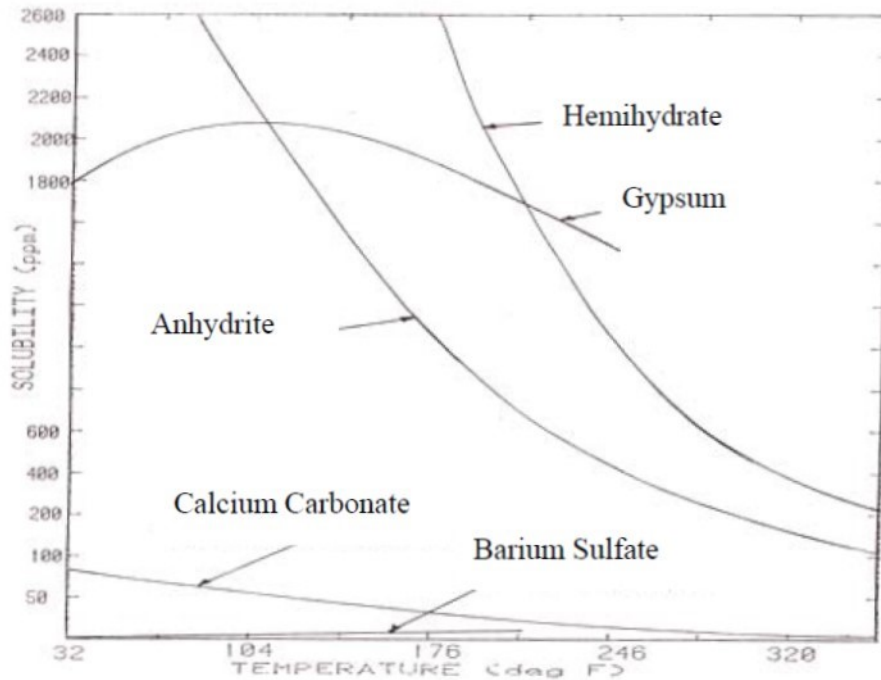


Figure 2.4: Mineral scale solubilities (ppm) *versus* temperature (F). [27]

the calcium carbonate and ferrous Carbonate.

In calcium carbonate scale prediction its relevant to account for the fugacity and the partitioning of CO_2 [32]. The fugacity and partitioning of the CO_2 will increase the complexity of the calculations but will assure an accurate estimation in terms of calcite saturation index and pH. As can be seen in Figure 2.5 there is a strong dependence of pH in what concerns the equilibrium of CO_2 , HCO_3^- and CO_3^{2-} .

The main equations governing this equilibrium are as follows [22, 35, 41]:

1. The reaction of the CO_2 gas phase with water will originate carbonic acid, which will further dissociate to form bicarbonate ion, as can be seen in equation 2.3.1.



$$K_1 = \frac{\gamma H^+ [H^+] \times \gamma HCO_3^- [HCO_3^-]}{CO_2}, \quad (2.3.2)$$

where K is the ionization constant, γ represents the activity of the component and the square brackets represent the concentration in moles per liter.

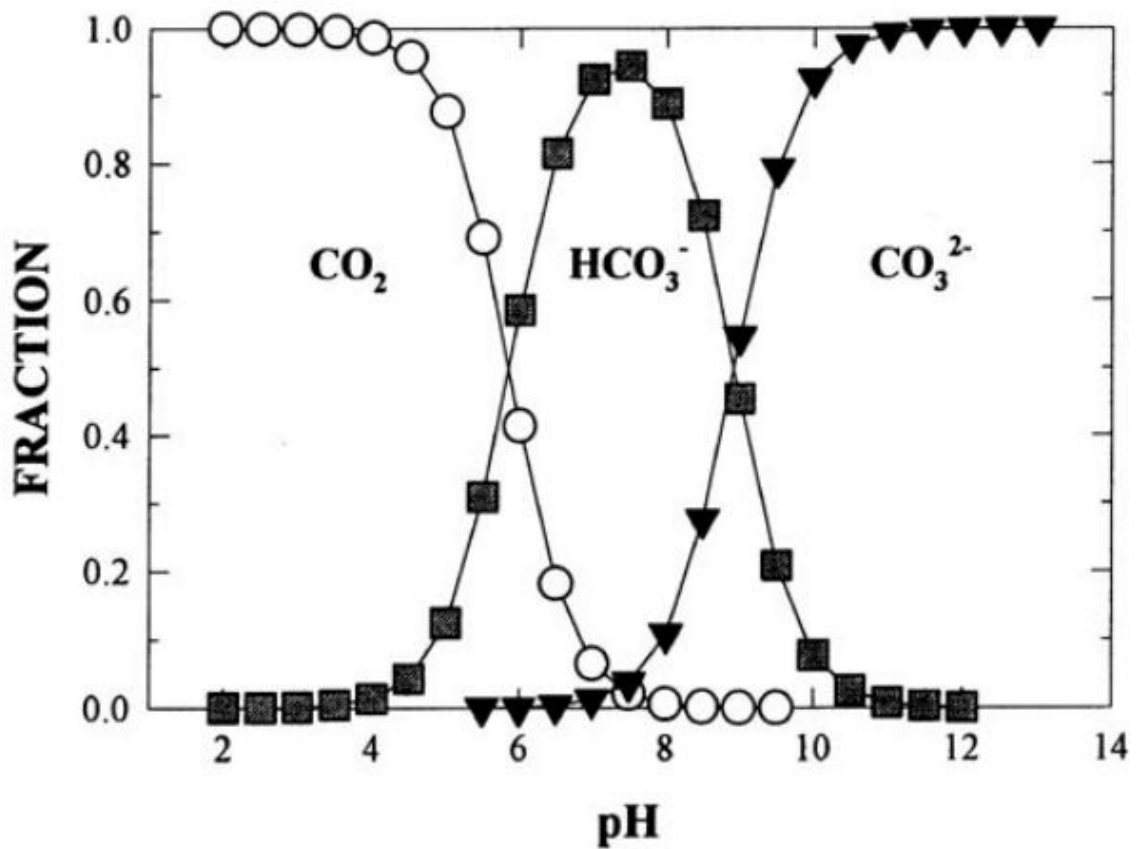


Figure 2.5: Carbon dioxide, bicarbonate and carbonate ions equilibrium dependence on pH for various fractions of carbonic acid in seawater. Source [4].

2. Also, the bicarbonate ion dissociates to generate carbonate ion as one can see in the following equation 2.3.3:



$$K_2 = \frac{\gamma H^+ [H^+] \times \gamma CO_3^{2-} [CO_3^{2-}]}{\gamma HCO_3^- [HCO_3^-]}, \quad (2.3.4)$$

where, similarly to the equation 2.3.2, K is the ionization constant, γ represents the activity of the component and the square brackets represent the concentration in moles per liter.

3. The formation of carbonate scales is originated when the carbonate and bicarbonate ions react with divalent cations, such as Ca^{2+} (see equations 2.3.5 and 2.3.8) [41].

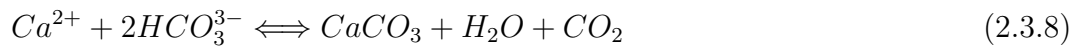


$$K_3 = \gamma Ca^{2+} [Ca^{2+}] \times \gamma CO_3^{2-} [CO_3^{2-}], \quad (2.3.6)$$

where, once again, K is the ionization constant, γ represents the activity of the component and the square brackets represent the concentration in moles per liter.



4. The entire equilibrium process is described by the following reaction [41]:



Moreover, besides the strong link to the pH of the fluid, as previously mentioned, there is also an interdependence with the temperature and pressure of the system. As a general trend, one can say that calcium carbonate is characterized by inverse solubility, meaning that, the rise in temperature promotes the precipitation of $CaCO_3$, *i.e.*, there will be carbonate scale formation with increasing temperature trends [4]. One of the most common

causes of carbonate scale formation is linked to pressure drops, specifically if the pressure decreased below the bubble point pressure of the CO_2 , leading to its release from the solution into the gas phase. [41]

For future reference, if there is presence of a gas phase, one should implement the following equations in order to calculate the calcite saturation index (SI) and pH for oil and gas wells [32]:

$$SI = \log \left[\frac{(Ca^{2+})(HCO_3^-)^2}{P y_g^{CO_2} f_g^{CO_2}} \right] + 5.85 + 15.19 \times 10^{-3}T - 1.64 \times 10^{-6}T^2(\dots) \quad (2.3.9)$$

$$(\dots) - 5.27 \times 10^{-5}P - 3.334(IS)^{\frac{1}{2}} + 1.431(IS),$$

where SI is the saturation index, (Ca^{2+}) is the total calcium (M=mg/l ÷ 40000), (HCO_3^-) is the bicarbonate alkalinity (M=mg/l ÷ 61000), P is the total absolute pressure in psia, $y_g^{CO_2}$ is the mole or volume fraction of CO_2 in the gas phase at the specified T and P, $f_g^{CO_2}$ is the fugacity coefficient as a minor species in $CH_4 + CO_2$ gas, T is the temperature in °F and IS is the ionic strength in mg/l.

$$pH = \log \left[\frac{(HCO_3^-)}{P y_g^{CO_2} f_g^{CO_2}} \right] + 8.60 + 5.31 \times 10^{-3}T - 2.253 \times 10^{-6}T^2(\dots) \quad (2.3.10)$$

$$(\dots) - 2.237 \times 10^{-5}P - 0.990(IS)^{\frac{1}{2}} + 0.658(IS),$$

where the notations previously described for equation 2.3.9 apply.

$$f_g^{CO_2} = \exp \left[P(2.84 \times 10^{-4} - \frac{0.255}{T + 460}) \right], \quad (2.3.11)$$

where $f_g^{CO_2}$ is the fugacity coefficient as a minor species in $CH_4 + CO_2$ gas and T is the temperature in °F.

$$y_g^{CO_2} = \frac{y_t^{CO_2}}{\left[1.0 + \frac{P f_g^{CO_2} (5.0BWPD + 10.0BOPD) \times 10^{-5}}{MM_{scf}(T+460)} \right]}, \quad (2.3.12)$$

where $y_g^{CO_2}$ is the mole or volume fraction of CO_2 in the gas phase at the specified T and P, $y_t^{CO_2}$ is the mole or volume fraction of CO_2 considering gas plus oil plus brine ("essentially

is the fraction of CO_2 in the gas at surface, $BWPD$ is the barrels of brine produced per day, $BOPD$ is the barrels of oil produced per day and the MM_{scf} is the total number of million cubic feet per day of produced gas at standard P and T (normally set at 60°F and 14.7 psia).

Sulfate Scales

Regarding the sulfate scales, similarly to the carbonate scales, predictive equations to calculate the saturation indexes for the mineral scales containing Ca^{2+} , Sr^{2+} and Ba^{2+} have been developed and can be found in [32].

The formation of sulfate scales is generally correlated to the incompatibility phenomenon due to the mix of formation water and seawater, the first containing divalent cations and the second characterized by high content of sulfate ions.

For a regional scale, one can say that barium sulfate and strontium sulfate scale mostly occur associated to sandstone formations, on the other hand calcium sulfate scales are mostly found in connection with limestone formations [41]. Barium sulfate is the most insoluble scale and a major concern in oilfields. Its origin is generally associated with the mixture of two incompatible waters that follow workovers or reservoir flooding. In most cases "the solubility of barium sulfate goes up with increasing temperature, pressure and salt content of the brine." [27]

The fundamental parameter interfering in the chemical equilibrium of sulfate mineral is the temperature (low temperatures and favorable to the precipitation of sulfate minerals [41]). Also, the total dissolved solids and pressure may condition the scale forming phenomenon. The pH variation has very small or no effect.

The calcium sulfate scale can occur in several crystallographic forms essentially depending on the temperature conditions and ionic strength, as follows [27]:

1. Gypsum: the most common. Occurs at low temperatures;
2. Anhydrite: frequent for temperatures above 100°C;
3. Hemihydrate: known to appear in presence of non-turbulent and high ionic strength conditions for a temperature range of 100-121°C.

As a general note, the calcium sulfate scale shows decreasing solubility with increasing temperatures, especially above 40°C. [27]

Exotic scales: other scale types

Apart from the well known carbonate and sulfate scale minerals, there are some other minerals which occurrence is comparatively rare, therefore here called exotic scales, although its potential to cause scale issues might be moderate-high depending on the site physicochemical conditions.

One example is the formation of sulfide scales, which occur due to fluid incompatibilities related to the exposure of hydrogen sulfide gas to iron, zinc or lead rich formation waters. The mineral precipitation follows the equation [5]:



Another example is the silica-based scales that occasionally form in oil-producing formations. Like the alkaline earth metal scales, such as $BaSO_4$, $SrSO_4$ and $CaSO_4$, these scales are water-borne and highly insoluble. The most frequently encountered silica-based scale is potassium fluorosilicate. [40]

2.3.3 Scale Prevention and Treatment

The water injection in the reservoir is associated to multiple proven benefits, namely: a) for pressure maintenance, which avoids subsidence problems and b) for an efficient reservoir sweep, which leads to a production increase. However, if the water injection process is not carefully evaluated and planned it can lead to severe operation problems, formation damage and even complete production loss. [29]

Scale Prevention

In order to prevent or mitigate scale formation, there is the need of continuous control of the chemical and physical conditions at the injection wells, at the near well-bore region, in production tubing and production facilities. This control is related to a number of variables, namely:

1. Prevention of the occurrence of supersaturation conditions;
2. Ionic control of the injected waters;

3. Reservoir injection of scale inhibitors;
4. Pressure control.

The first and second above-mentioned factors are partially interlinked and are extremely important if there is a possibility of incompatibility of waters. In brief, this would involve in depth chemical studies + laboratory testing of the reservoir formation water and possible sources of injection water for a specific reservoir or for example membrane filtration, in order to remove undesirable ions, similarly to what is done in sulfate removal plants (SRP) in which the sulfate present in seawater is retained in the membranes.

Scale inhibition can correspond to dilution methods or to addition of scale inhibitor chemicals [8]. The scale inhibitors can vary from the so-called chelating inhibitors, which avoid scale formation (to a limited level of oversaturation) by "consuming scale ions in stoichiometric ratios" to the so-called threshold scale inhibitors, which chemically interact with the crystal nucleation sites and decrease the crystal growth rates. [8] There are numerous scale inhibitors available in the market, some can even be injected into the reservoir in an encapsulated form allowing the chemical to be delivered over an extended period of time [39]. In terms of chemical nature most of them correspond to phosphate compounds, such as, inorganic polyphosphates, organic phosphate esters, organic phosphonates, organic aminophosphates and organic polymers [8].

Scale Treatment

The scale removal generally takes place when there is flow restriction and notorious loss in production. Essentially, there are two main mechanisms for scale removal [41]: a) Chemical dissolution and b) Mechanical removal.

The chemical techniques for scale treatment are generally the first option to be deployed in case of scale problems, since they are often less expensive compared to the mechanical methods. These can be done by a stimulation vessel, in an operation called scale squeeze. The mechanical techniques normally involve the placement of a workover rig (in offshore wells) and the use of various tools, such as, brushes, string-shots, mill, which are introduced into the well by wireline or coiled tubing. [8, 41]

2.4 Analytical Techniques

In current section the main features of the analytic methods used for this work will be briefly described.

2.4.1 Inductively Coupled Plasma - Optical Emission Spectrometry (ICP-OES)

The ICP-OES (Inductively coupled plasma - optical emission spectrometry) is a technique in which the sample composition can be determined [42]. The ICP-OES schematic representation can be seen in Figure 2.6, which shows the major components of the analytical instrument. An aqueous sample is conducted by a peristaltic pump to the analytical nebulizer. The sample aerosol is led into an argon plasma flame. In the ICP-OES the plasma is generated at the end of a quartz torch by a cooled induction coil through which a high frequency alternate current flows. As a consequence, an alternate magnetic field is induced favoring the circular trajectory of accelerated electrons. Due to collision between the argon atom and the electrons ionization occurs, giving rise to a stable plasma. In order to the sample composition to be determined the sample droplet will be exposed to a sequence of processes, as follows: desolvation, vaporization, atomization and ionization. [7]

Due to the thermic energy taken up by the electrons, they reach a higher energy level (excited state). Once the electrons decay to the low energy state, the element characteristic radiation is emitted and detected by a spectrometer. The radiation intensity for each wavelength is measured and converted into element concentration. [7, 42]

2.4.2 Ion Chromatography (IC)

Ion chromatography is a chromatography process in which the separation is based on ionic (or electrostatic) interactions between ionic and polar analytes, ions present in the eluent and ionic functional groups fixed to the chromatographic support [45]. There are two types of ion chromatography : a) anion-exchange; b) cation-exchange (used when the molecule of interest is positively charged). For the purpose of this study, only the anion-exchange ion chromatography was used and its principle will be further explained. In anion-exchange

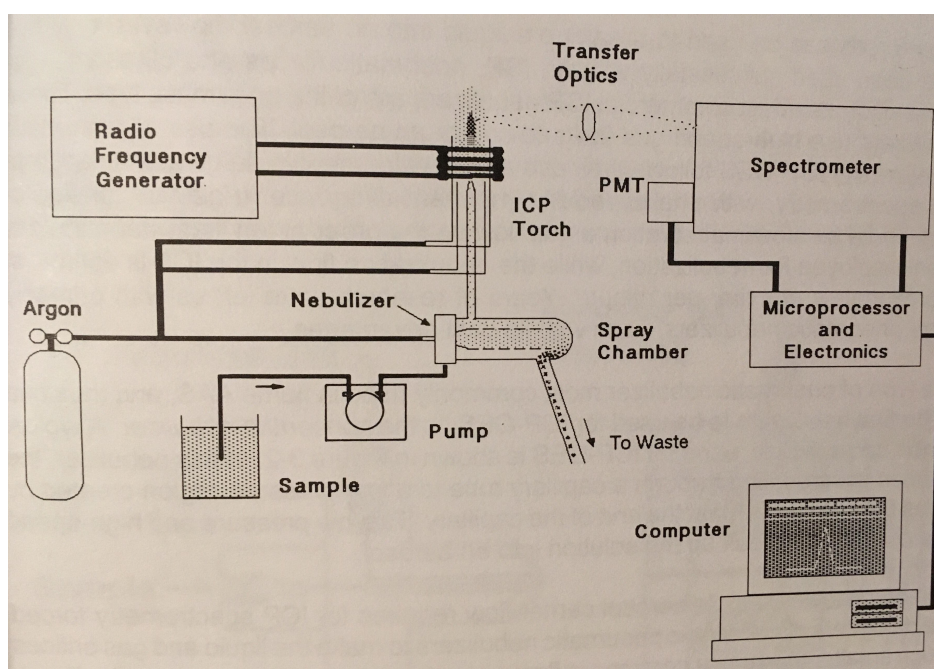


Figure 2.6: Major components and layout sketch of a typical ICP-OES. PMT stands for photomultiplier tube. Source [7].

chromatography the stationary phase is positively charged and the sample containing negatively charged ions is loaded and passed through it to be attracted. Afterwards, the bound molecules are eluted and collected using an eluent. In order for the elution to occur it is required to alter the condition, by either increasing the concentration of the exchangeable counter-ions, which competes with the molecules for binding or modifying the pH. It relevant to further clarify that "a change in pH affects the charge on the particular molecules and, therefore, alters binding. The molecules then start eluting out based on the changes in their charges from the adjustments." [30]

Figure 2.7 shows a diagram of the various components integrating the ion chromatography analyzer. It is relevant to mention that the used apparatus is constituted by one-channel only.

2.4.3 Gas Chromatography with Flame ionization Detector (GC-FID)

The gas chromatography coupled with FID (GC-FID), is a variant of the normal gas chromatography, "that is well suited for analysis of hydrocarbons such as methane, ethane, acetylene etc., but also for organic substances containing hydrocarbons and for volatile

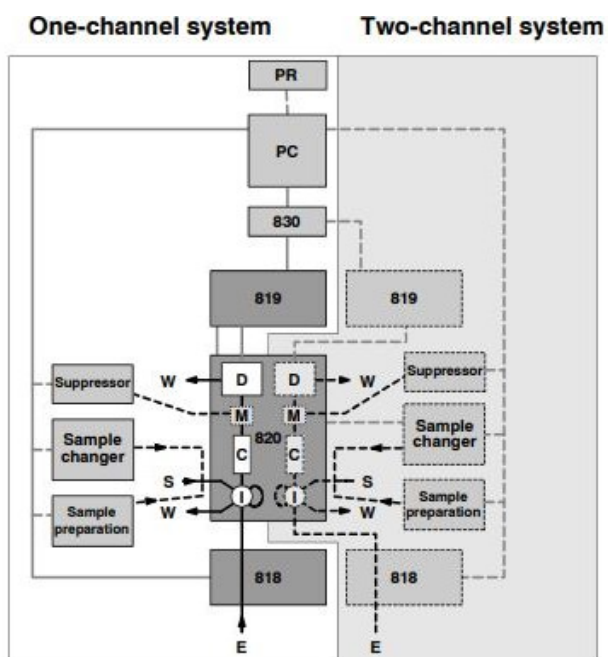


Figure 2.7: Block diagram of the ion chromatography systems, in which C: Separating column; D: Detector; E: Eluent; I: Injector; M: Suppressor Module; PC: computer; PR: Printer; S: Probe; W: Waste; 818: IC pump; 819: IC detector; 820: IC Separation center and 830: IC interface. Source [18].

organic compounds (VOCs)" [2]. In GC the different chemical constituents of a sample pass in a gas stream, the carrier gas (He) at different rates depending on their chemical and physical properties and interaction with a specific the GC column. The detection of the various chemical compounds is made as they exit the GC column and its identification is controlled by the exhibited retention times.

"In an FID the sample undergoes a combustion in a hydrogen/synthetic air flame. Ions and free electrons are formed in the flame. The charged particles produce a measurable current flow in the gap between two electrodes in the detector. The resulting current flow is of greater strength than the signal produced by the pure carrier gas and the fuel gas flame alone. This signal differential provides information about the sample. The current is proportional to the information which depends on the composition of the separated sample." [2] The Figure 2.8 illustrates the various components present in the GC-FID.

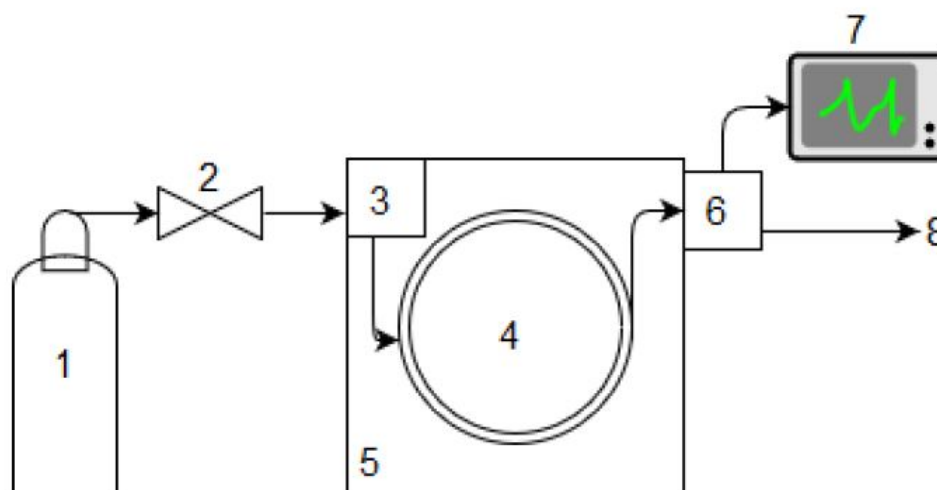


Figure 2.8: Schematic representation of the GC-FID equipment, in which 1: Gas carrier; 2: Flow controller valve; 3: Injector port; 4: Column; 5: Thermostatic oven; 6: Detector (FID); 7:Recorder and 8: Waste line for gathering of paralyzed products. Courtesy of Mathias K. Jørgensen.

2.4.4 Total Carbon (TC)

The total carbon (TC) analysis encompasses the measurement of both the totality of carbon present in the sample and the inorganic carbon (IC or TIC). The total organic carbon, TOC, is later on estimated by the subtraction of the inorganic carbon from the

total carbon.

The TC methodology is characterized by four main steps: a) the acidification: the inorganic fraction of carbon is converted to CO_2 ; b) the oxidation: all remaining carbon is converted into CO_2 due to high temperature combustion; c) Detection and d) Quantification. [43]

2.4.5 X-ray Fluorescence (XRF)

X-ray fluorescence (XRF) is an analytical non-destructive technique that allows the user to obtain the elemental composition of rocks, minerals, sediments and fluids. The preparation of samples for XRF analysis is economic, and the stability and ease to use x-ray spectrometers makes this technique one of the most widely used methods for analysis of major and trace elements [44]. The XRF principle states that "individual atoms, when excited by an external energy source, emit X-ray photons of a characteristic energy or wavelength. By counting the number of photons of each energy emitted from a sample, the elements present may be identified and quantified" [14].

The sample is illuminated by an intense X-ray beam; some of the energy is scattered, but some is also absorbed within the sample in a manner that depends on its chemistry. The incident X-ray beam source is generally Rh, although W, Mo, Cr and others can also be used, depending on the application [44]. In current case the x-ray source beam is Pd.

"The primary X-ray beam illuminates the sample, it is said to be excited. The excited sample in turn emits X-rays along a spectrum of wavelengths characteristic of the types of atoms present in the sample. Essentially, the atoms in the sample absorb X-ray energy by ionizing, ejecting electrons from the lower, usually K and L, energy levels. The ejected electrons are replaced by electrons from an outer, higher energy orbital. When this happens, energy is released due to the decreased binding energy of the inner electron orbital compared with an outer one. This energy release is in the form of emission of characteristic X-rays indicating the type of atom present" [44].

3 Experimental Work

3.1 Experimental Materials and Techniques

The current experimental work aims to investigate the mineral scaling associated to the produced water injection. In order to achieve this goal, two main laboratory experiments were carried out: a) beaker test and, b) coreflooding.

3.1.1 Rock samples

In this experimental investigation two different rock samples were used. Dan chalk, kindly provided by DanKalk K/S has its origin in Denmark. Austin Chalk, has its origin in the Austin Chalk formation (Texas, USA). The chemical compositions of the two above-mentioned rock samples was obtained using an Rigaku supermini 200 X-ray fluorescence (XRF) analyzer (see Table 3.1).

3.1.2 Formation and Produced water samples

Current work has focused on the scale potential linked to the injection of produced water into the reservoir, therefore is important to use an offshore sample of produced water that has been taken at the wellhead, meaning that no treating chemicals have been added. The offshore wellhead sample has been kindly provided by MÆRSK OLIE OG GAS A/S a TOTAL S.A Company.

An offshore wellhead sample is a mixture of oil, gas and produced water; therefore, there was the need to separate and decant the produced water to further use it in the experiments.

Table 3.1: Dan Chalk and Austin Chalk chemical compositions. Results provided by XRF analysis.

Component	Dan Chalk [mass%]	Austin Chalk [mass%]
CaO	95.3	95.4
MgO	-	1.22
Al_2O_3	0.439	0.355
SiO_2	3.30	1.75
P_2O_5	0.346	0.176
K_2O	0.127	-
SrO	0.432	0.098
Fe_2O_3	-	0.510
SO_3	0.0591	0.132
Cl	0.0125	0.039
Total	100.016	99.680

The Formation waters used were synthetic Ekofisk formation water (EFW) and synthetic Valhall formation water (VFW). These have been prepared based on published chemical compositions (Table 3.2) [38, 10] following the experimental procedure, which has a reference volume of 1 liter and room temperature, as follows:

1. Chloride salts are diluted in ca. 400 ml of deionized water (DI) water;
2. Sulfate salts are diluted in ca. 200 ml of DI water;
3. Carbonate salts are diluted in ca. 200 ml of DI water;
4. The brines (*s.l.*) are mixed into a volumetric flask and the remaining 200ml of DI water are added;
5. The solution is stirred until the salts are fully dissolved.

3.1.3 Analytical Techniques

In current research work various analytical methods have been used essentially to evaluate the chemical changes linked to the brine (*s.l.*)–rock interactions. Additionally, the oil in water for the produced water was measured.

Table 3.2: Ekofisk Formation Water and Valhall Formation water chemical compositions.

Chemical components	EFW	VFW
	Concentration (g/l)	Concentration (g/l)
<i>NaCl</i>	67.3	57.6
<i>Na₂SO₄</i>	-	0.1
<i>NaHCO₃</i>	0.332	0.75
<i>KCl</i>	0.549	0.35
<i>MgCl₂ x 6H₂O</i>	4.45	1.6
<i>CaCl₂ x 2H₂O</i>	14.69	4.3
<i>BaCl₂ x 2H₂O</i>	0.45	-
<i>SrCl₂ x 6H₂O</i>	2.27	-
TDS	90.041	64.7

Inductively Coupled Plasma - Optical Emission Spectrometry (ICP-OES)

The Inductively Coupled Plasma - Optical Emission Spectrometry (ICP-OES) was used to measure the concentrations of metals in produced water prior and after flooding the core sample. All results were gathered with Perkin Elmer - Optima 8000 instrument, following the procedure described below:

1. Build a method to measure the concentration of the metals of interest. For the purpose of the current experimental method Ca, Sr, Na, Mg, Ba, Fe, Zn and K were selected. The wavelengths selected for each metal can be seen in Table 3.3;
2. Build a sample list and select a wash time of 90 seconds and 3 replicates for each sample;
3. Run a calibration blank;
4. Run the calibration standards for multi-element concentrations 0.2 mg/l, 1mg/l, 5mg/l and 10mg/l. Note that in these reference materials the K concentration is 10 times higher the referred value;
5. Check if the calibration curves are providing the correct concentrations and correct them if necessary. Save method;
6. Run a blank sample;

7. Analyze the samples.

Table 3.3: Metals wavelengths (nm) analyzed in ICP-OES measurements.

Metals	Wavelengths (nm)
Ba	233.527
Fe	238.204
K	766.49
Mg	279.553
Na	589.592
Zn	213.857
Sr	421.552
Ca	317.933

Ion Chromatography (IC)

The ion chromatography was used in order to analyze the anionic concentration of the brines (*s.l.*). In current experimental work a 820 IC Separation center/819 IC Detector by Metrohm was used. The experimental procedure is composed by 4 steps:

1. Preparation of the Eluent:

- a) Weigh 84 mg of $NaHCO_3$ and save it for later usage;
- b) Weigh 339 mg of Na_2CO_3 and keep it for later use;
- c) Add both salts into an 1 liter volumetric flask and put it to stir for at least 30 minutes.

Note: The eluent will lose its properties in approximately 3 days, therefore it should be renewed even if not fully consumed.

2. Preparation of the regeneration liquid for the suppressor:

- a) prepare a solution with 0.1 M of H_2SO_4 and add it to a 1 liter flask. Make sure that there is always at least 200 ml of regeneration liquid in the flask before starting measurements.

3. Preparation of the standards for calibration:

- a) Use the certified standard – IC Multi-Element Standard, 7 Elements by Reagecon (see [37] for the quality sheet) to prepare the standards 1, 2 and 3;
- b) Prepare standard 3 by taking 5ml of the certified standard and pour it into a 50 ml volumetric flask and fill it with distilled water;
- c) Prepare standard 2 by taking 25 ml of the standard 3 and pour it into a 50 ml volumetric flask and fill it with distilled water;
- d) Prepare standard 1 by taking 25 ml of the standard 2 and pour it into a 50 ml volumetric flask and fill it with distilled water.

Table 3.4: Concentration of the standards 1,2 and 3 for ion chromatography.

Anions	F^-	Cl^-	NO_2^-	Br^-	NO_3^-	PO_4^{3-}	SO_4^{2-}
Standard 1	0.50	2.50	2.50	2.50	2.50	5.00	2.50
Standard 2	1.00	5.00	5.00	5.00	5.00	10.00	5.00
Standard 3	2.00	10.00	10.00	10.00	10.00	20.00	10.00

4. Samples preparation and analysis:

- a) Take approximately 10 ml of the sample to analyze and filtrate it with 0.45 μ m filter;
- b) Add the filtered sample into a clean vial;
- c) Set-up the auto-sampler, run the calibration standards, verify if the peaks and concentrations match the standards and correct if necessary;
- d) Analyze the samples.

Gas Chromatography with Flame ionization detector (GC-FID)

In current experimental work, the Gas chromatography with flame ionization detector (GC-FID) was used in order to estimate the oil content present in the produced water (OIW). A Perkin Elmer Clarus 680 with a built-in auto-sampler was used to perform the OIW measurements. The procedure to determine the OIW is a variation of the OSPAR reference method and can be described as follows:

1. *Sample Preparation: Liquid-liquid extraction using n-hexane as solvent.*

Table 3.5: IC Multi-Element Standard– 7 Elements: Concentration and QC [37]

Anion	Raw Material Purity %	Nominal mg/L	Actual mg/L
Fluoride	99+	20.0	20.05
Nitrite	99+	100	100.1
Nitrate	99+	100	99.9
Phosphate	99+	200	200.1
Sulphate	99+	100	100.1
Bromide	99+	100	99.9
Chloride	99+	100	100.4

- a) Weigh 30g of aqueous phase and 10 g of n-hexane;
- b) Add the aqueous phase and n-hexane in a 100 ml separation funnel;
- c) Shake it vigorously for approximately 2 minutes;
- d) Allow the mixture to settle and separate (in the specific case ca. 5 minutes of settling time);
- e) Once a clear interface has formed, a syringe is used to extract a sample of the organic phase (the upper phase).
- f) Weigh the organic phase sample. The weight of the organic sample will be dependent on the residence time, but it should be in the range of 1–3 g.
- g) Decant the aqueous phase and the remaining organic phase separately and weigh them.

2. GC-FID Determinations and Results analysis

- a) Prepare the standards. In current experiment the calibration curve was obtained for the following range of concentration: 200–1200 ppm (Figure 3.1).
Note: If the calibration shows an R^2 below 0.985 discard the calibration and repeat the procedure;
- b) Analyze the samples. Ensure that three replicates will be measured;

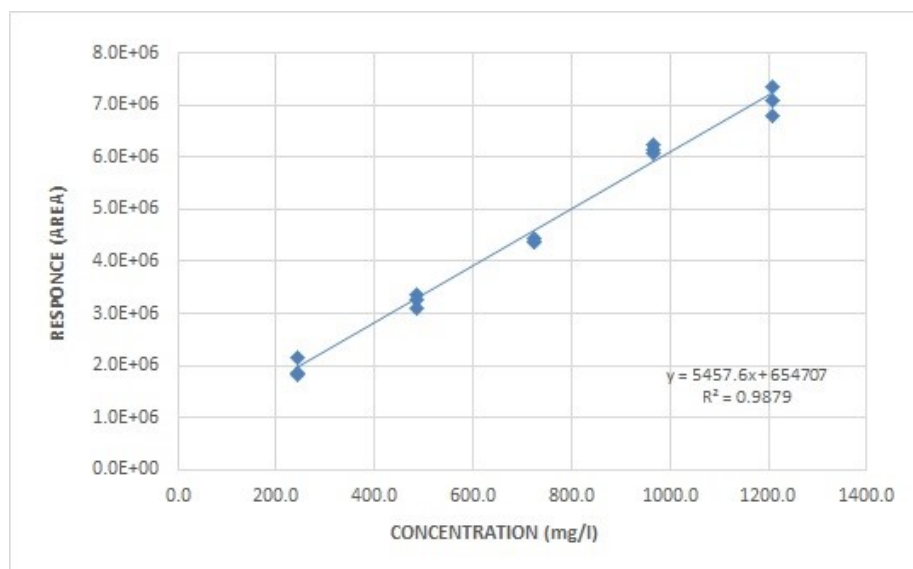


Figure 3.1: Calibration curve for crude-oil. Courtesy of Mathias K. Jørgensen.

- c) Analyze the chromatogram and calculate the average value for the response area. The response area is provided in $\mu\text{V}\cdot\text{sec}$.
- d) Use the calibration curve to calculate the concentration of OIW.

Total Carbon (TC)

The total carbon was used in order to determine the concentration of the organic and inorganic carbon present in each sample. An Analytik jena multi N/C 2100 analyzer was used for the measurements. The procedure was as follows:

1. Prepare the samples and pour them into the vials. These should be sterilized.
2. Prior to start the equipment :
 - a) Verify if the O_2 pressure to 4.5 bar, if not set it to 4.5 bar;
 - b) Check if there is enough phosphoric acid (H_3PO_4) for the defined number of measurements. Note that each measurement will take ca. 0.5ml of liquid .
3. Start the TC analyzer and allow it to run for ca. 30 minutes. Check if the equipment is ready (all devices should appear blue or black in the "status window").
4. Prepare the standards. See the standards concentration in Table 3.6.

5. Create or load an adequate method and check if the analyzer is properly calibrated by analyzing 3 standards as samples and checking if the results are satisfactory;
6. If the results fit the method calibration, proceed and analyze the samples. If not, calibrate the equipment.
7. Ensure that three replicates are acquired for each sample.

Table 3.6: Standard concentrations in mg/l for the total carbon analyzer.

<i>Standards</i>	<i>Concentration : TC- TIC (mg/L)</i>
1	500 mg TOC/l – 250 mg TIC/l
2	250 mg TOC/l – 125 mg TIC/l
3	100 mg TOC/l – 50 mg TIC/l
4	50 mg TOC/l – 25 mg TIC/l
5	25 mg TOC/l – 12,5 mg TIC/l
6	10 mg TOC/l – 5 mg TIC/l
7	5 mg TOC/l – 2,5 mg TIC/l

X-ray Fluorescence (XRF)

In current experimental work one intend to compare the elemental composition of two chalk samples, one with origin in the North Sea (Dan chalk) and the second one in Texas, USA (Austin Chalk). An X-ray fluorescence analyzer, Rigaku supermini 200 was utilized, following the procedure described below:

1. Prepare a sample vial using polyethylene film and weigh it;
2. Weigh ca. 1 g of sample powder and add into the vial and put on the lid. Make sure that the entire bottom of the vial is covered with powder.
3. Place the sample vial into the sample holder;
4. Initiate the XRF analyzer and wait 30 minutes for the spectrometer to initialize and the calibration to run;
5. Analyze the sample.

3.1.4 Beaker Test

The beaker test intends to understand the chemical interaction of chalk with different formation water and produced water, by investigating the pH variation associated with this chemical process. The experiment was performed for room temperature (23°C) and 70°C. The rock sample used is Dan chalk, which is a very pure limestone, as described in section 2.1.1. Its chemical composition can be seen in the table 3.1.

The beaker test was initially thought and designed to be performed at two variations. Due to time constrain, the experimental results were exclusively acquired for variation A. Both experimental procedures are described as follows:

1. Variation A:

- a) Use a 100 ml glass autoclave bottle and fill it with 60 ml of produced water or formation water.
- b) Measure the initial pH. This pH will be pH_0 .
- c) Take a chalk sample with rough edges (this should fit the opening of the glass bottle), remove the excess of chalk powder and measure and register its weight;
- d) Insert the chalk sample in the glass autoclave bottle (Figure 3.2) and tighten the lid. Let the chalk sample age in the glass bottle for 24 hours at the predetermined temperature.
- e) Untighten the lid and measure the pH. This will be pH_{24} (Figure 3.3).
- f) Tighten the lid again and age the chalk sample for 10 days at the selected temperature.
- g) Remove the lid and measure the pH. This will be pH_a .
- h) Put the lid back and age the sample for 24h at the selected temperature.
- i) Open the glass autoclave and measure the pH. This will be pH_x , in which x is the following number on the pH measurements.
- j) Repeat the steps h) and i), until constant pH value is found.

2. Variation B:

- a) Get a 100 ml glass autoclave bottle weigh it (W1) and fill it with 60 ml of formation water.
- b) Measure the initial pH of the formation water. This pH will be pH_0FW .
- c) Take a chalk sample with rough edges (this should fit the opening of the glass bottle), remove the excess of chalk powder and register its weight;
- d) Insert the chalk sample in the glass autoclave bottle, weigh it (W2) and tighten the lid. Let the chalk sample age in the glass bottle for 24 hours at the predetermined temperature.
- e) Untighten the lid and measure the pH. This will be pH_{24FW} .
- f) Keep measuring the pH each 24h until the pH has reached a stable value.
- g) Pour out all the formation water and weigh the autoclave bottle with the saturated chalk sample inside (W3).
- h) Fill the glass autoclave bottle with 60 ml of produced water.
- i) Let the saturated chalk sample age in the glass bottle for 24 hours at the predetermined temperature.
- j) Untighten the lid and measure the pH. This will be pH_{0PW} .
- k) Tighten the lid again and age the chalk sample for 24h at the selected temperature.
- l) Remove the lid and measure the pH. This will be pH_{24PW} .
- m) Put the lid back and age the sample for 24h at the selected temperature.
- n) Open the glass autoclave and measure the pH. This will be pH_{axPW} , in which "ax" is the number of days after the initial pH measurement.
- o) Repeat the steps m) and n), until constant pH value is found.
- p) Pour out the excess of produced water inside the glass autoclave bottle and weigh it (W4).

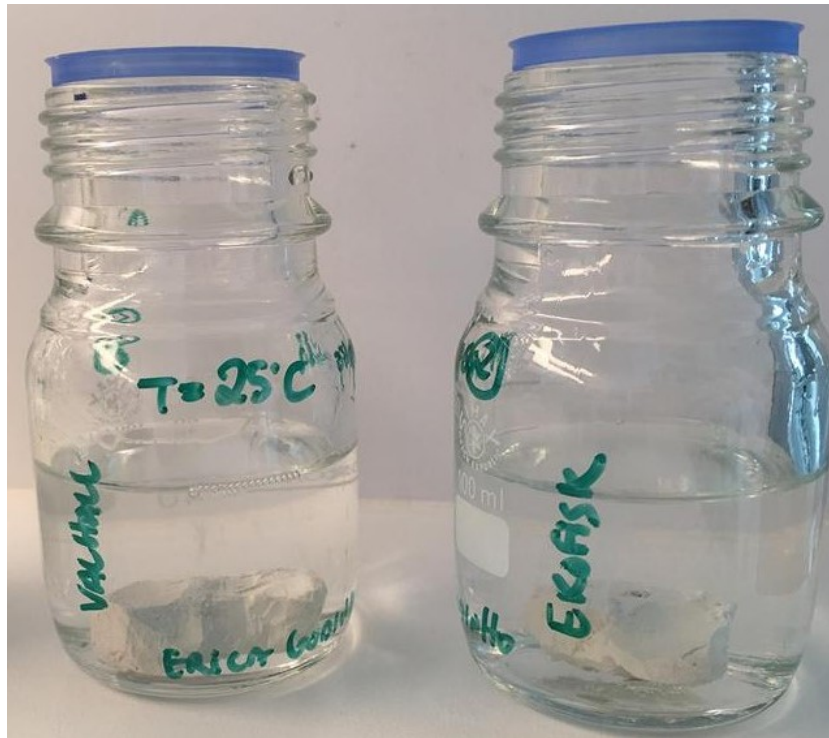


Figure 3.2: Preparation of the autoclave flask with the chalk and selected brine (*s.l.*).

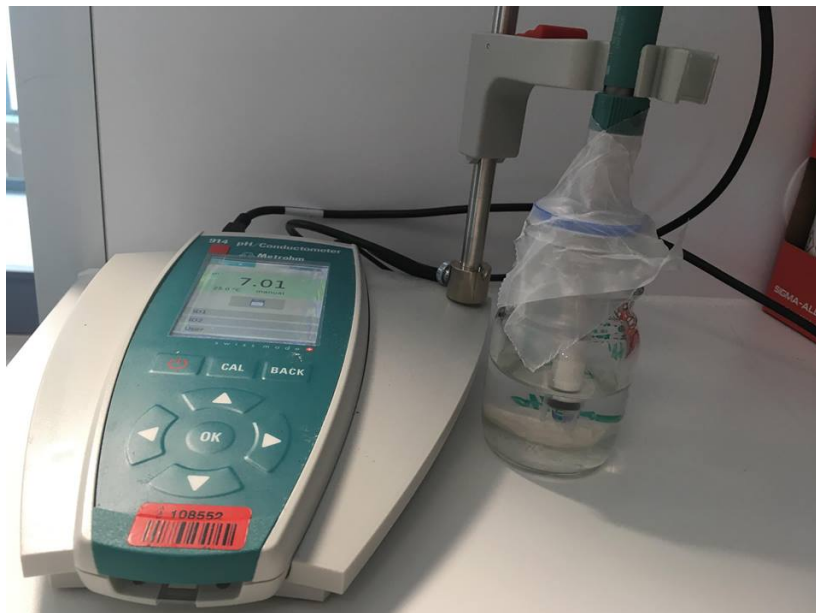


Figure 3.3: pH measurement of the brine (*s.l.*) after 24h of exposure to the rock.

3.1.5 Coreflooding Analysis

The coreflooding technique has been used to get a quantitative estimation of the permeability and porosity variation associated to produced water injection. Mainly, in current study one intended to investigate the incompatibility associated to the mixture of brines (*s.l.*) at constant reservoir temperature, constant flow-rate and increasing pressure.

Porosity and permeability measurements

The core tests require the knowledge of the initial state of the core sample, therefore a AP-608 Automated Permeameter-Porosimeter by Coretest systems, Inc. was used. "The AP-608 is a cost-effective advanced system for performing automated permeability and porosity tests at confining pressures up to 9950 psi over a wide permeability range. The AP-608 uses a pressure decay technique to determine Klinkenberg-corrected permeabilities, slip and turbulence correction factors"[17]. In order to obtain the porosity and permeability measurements the below procedure should be followed:

1. Measure and register (Table 3.7) the length and diameter of the core sample;
2. Weigh the dried core sample and register its weight (Table 3.7);
3. Verify the calibration of the equipment:
 - a) Use the 1.5 inches steel core and run the reference volumes test. If the test is passed proceed to the next step;
 - b) Run the leak check test, if passed proceed to the next step;
 - c) Use the 1.5 inches steel tube and run the calibration volumes test. If passed the equipment is ready to perform the porosity and permeability measurements.
 - d) Select "slow release" of the pressure;
4. Step up the equipment for the data acquisition:
 - a) Create a new file, input the length (cm), diameter (cm) and weight (g) of the core and click the option "calculate bulk volume";
 - b) Select measurement of 3 or 5 pressure sin the range 500–1000 psi.
 - c) Carefully place the core inside the core holder and adjust the top piston and bottom piece;

- d) Run the porosity a permeability measurements;
- e) For the results select to save "full job".

Table 3.7: Core samples data used in porosity and permeability measurements.

<i>Core Reference</i>	<i>Length (cm)</i>	<i>Diameter (cm)</i>	<i>Bulk Volume (cm³)</i>
AC2	7.621	3.744	83.90223371
AC3	7.632	3.752	84.38279425
AC4	7.627	3.739	83.74416527

Coreflooding

The coreflooding equipment is composed by a double pump plus pump controller connected to a 3-piston system (by Core lab). The 3-piston system is linked to the Hassler core holder (by Core lab), placed inside the oven, by a sequence of manually operated gate valves. The equipment is also composed by a back pressure regulator and a confining pressure pump and an effluent outlet. The inlet and outlet pressure, annulus pressure and core temperature are registered and controlled by pressure and temperature transmitters. The simplified representation of the coreflooding equipment can be seen in Figure 3.5. For pH measurements a 914 pH/conductometer by Metrohm was used; The coreflooding experimental procedure is constituted by two main steps, the core saturation (Figure 3.6 shows the saturation equipment) and the coreflooding itself and can be described as follows:

1. Saturation of the core:

- a) Fill the volumetric funnel with 1 liter of formation water;
- b) Place the dried core sample inside the desiccator and seal it;
- c) turn on the vacuum pump, connect the desiccator top valve to the outlet valve of the volumetric funnel;
- d) open the outlet valve and regulate the flow to be flowing drop by drop over the core sample;
- e) when all the fluid has been added into the desiccator, disconnect the volumetric flask from the top of it and close the valve at the desiccator;

- f) Allow the vacuum to work a fully extract the air (ca. 12-18 hours).
- g) open the desiccator, take the core sample out, dry the excess of water with paper towel and weigh the core sample. This will be the saturated weight.

2. Coreflooding Experiment:

- a) Place the core sample inside the Hassler type core holder;
- b) Set the oven temperature to the desired experimental temperature. In current experiment the temperature was set to 70°C;
- c) Turn on the pump controller and fill the pumps;
- d) Fill the piston A with injection fluid, in current case, produced water. Fill piston B with methanol and piston C with DI water;
- e) Purge the air in the system and pressurize the annulus using the confining pump; Note that the annulus P should be as stable as possible. By experience it was possible to regulate the valve and keep the P constant after ca. 1 or 2h from start of the experiment;
- f) Regulate the back pressure to 10 bar;
- g) Set the pump controller to constant flow-rate and select the desired flow-rate. In current experiment a flow-rate of 1 ml/min was applied;
- h) Open the valves at piston A and start the experiment and collect the effluent every hour and measure the pH; Note: The effluents should be kept isolated from the atmosphere.
- i) When the all the injection fluid has been pumped through the core sample and there is no more effluent the experiment is finished. Close the valves in piston A;
- j) Turn off the Pump controller, depressurize the annulus, and use the bleeding air valve to release any pressure from the inside of the coreholder;
- k) Turn of the oven and allow in to decrease the temperature until is possible to touch the core holder;
- l) Take the core sample from the inside of the core holder, dry the excess of water, if present, and weigh the core;

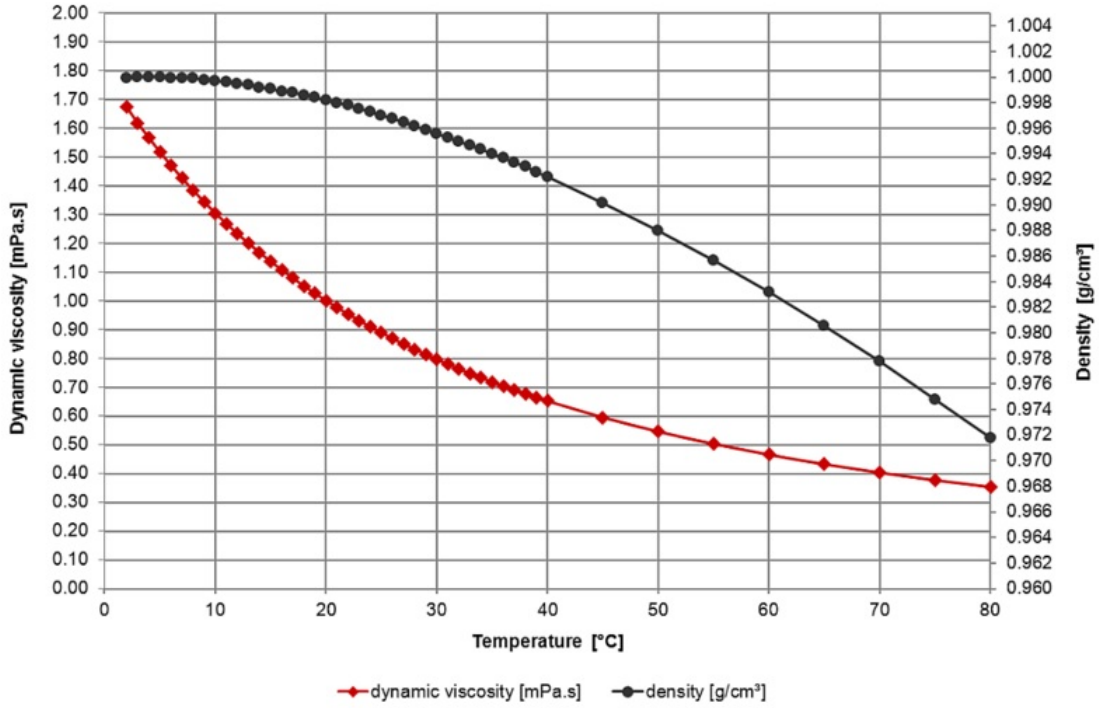


Figure 3.4: Pure water dynamic viscosity (cP) and density (g/cm^3) for various Temperatures. Source [34].

- m) When the experiment is finished, place the core in core holder and clean the core and system with methanol and DI water.

After the coreflooding results are gathered and cleaned, one calculated the permeability variation as a function of the differential pressure over time, following the so called Darcy's Law [3]:

$$Q = \frac{k \times A \times \Delta P}{\mu \times L}, \tag{3.1.1}$$

where, Q is the flow rate in cm^3/s , k is the permeability in darcies (D), A is the cross-sectional area in cm^2 , μ is the viscosity in centipoise (cP), L the length in cm and ΔP the pressure differential in atmosphere. The viscosity for the produced water was not possible to be experimentally measured as the viscometer apparatus doesn't allow viscosity measurements bellow 1 cP. Therefore, the author has decide to use the dynamic viscosity of pure water at 70°C as a reasonable estimation to be used for the permeability calculations. Such value is approximately 0.4035 cP, as can be seen in Figure 3.4.

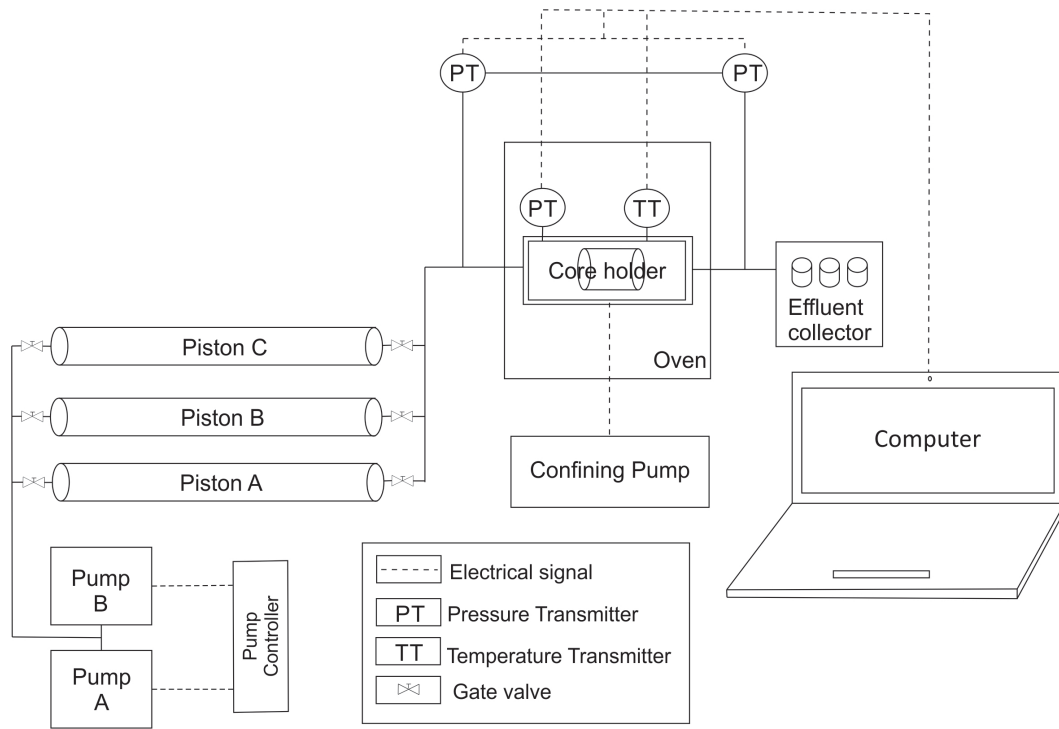


Figure 3.5: Simplified schematic representation of the coreflooding equipment.

The measured weight before and after the coreflooding experiments are presented in the Tables 3.8 and 3.9.

Table 3.8: Core sample dry and saturated weight before coreflooding experiments.

<i>Core Reference</i>	<i>Dry weight (g)</i>	<i>Saturated weight FW (g)</i>
AC2	167.08	184.93
AC3	163.07	183.09
AC4	159.37	179.21

Ionic concentration of the brines (*s.l.*)

As mentioned in chapter 2 there is an influence of the scaling potential of an electrolyte solution related to the ionic strength. This solution is characterized by the presence of positively charged cations and negatively charged anions, which were formed by the dissociation of chemical compounds when brought into solution. These ionic solids are held together by attractive electrostatic forces which act between cations and anions [11, 24].



Figure 3.6: Volumetric funnel and desiccator for core saturation.

Table 3.9: Core sample saturated weight after coreflooding experiments and core sample dry weight (exposure to 100°C) after coreflooding experiments.

<i>Core Reference</i>	<i>Saturated weight CF (g)</i>	<i>Dry weight CF (100°C)</i>
AC2	188.44	168.30
AC3	187.25	164.37
AC4	183.50	160.71

Calculation of the concentrations and ionic strengths stems from the general dissociation theory, which specifies that if an ionic solid is added to water, equilibrium between cations and anions is reached [16]. Generic calculation procedure for the ionic concentrations is as follows [10, 11]:

1. Knowing the molecular weight of particular salt and the amount of mass added to the solution, one can calculate the molarity;
2. According to the general dissociation theory, the amount of moles of each dissociated cation and anion is calculated;
3. The total amount of each cation and anion is summed;
4. TDS is equal to the sum of total amount of salts added to the aqueous phase.

Ionic strength is used to express the ionic composition of the solution. The following equation 3.1.2 is used to estimate the ionic strength:

$$\mu = \frac{1}{2} \sum_i c_i z_i^2, \tag{3.1.2}$$

where μ is the ionic strength in (mol/l) c_i is the concentration of the ion (mol/l) and z_i is the charge of the ion.

Note that, if one knows the ionic concentration in mg/l of all dissolved chemical species, the application of the equation 3.1.2 is direct after the conversion of units.

4 Results and Discussion

4.1 General Principles

Scale deposition of inorganic minerals is known to be a major trouble in oilfields. If not carefully taken care, this phenomenon can lead to huge operational costs, formation damage and safety issues.

This chapter will present the gathered results for the current research work. Various analytical techniques were used in order to understand the scale potential associated to the possible injection of produced water from the Halfdan field (North sea). For the experimental works, two chalk samples were used : Austin Chalk (USA) and Danchalk (DK), to reassemble the reservoir rock, once it was not possible to obtain a core sample from the same reservoir.

4.1.1 Beaker Test

The beaker test was performed for the Danchalk sample at atmospheric pressure and two different temperatures – 20°C and 70°C. Figure 4.1 illustrates the pH variation of the brines (*s.l.*) over one month experiment. Note that pH_0 refers to the initial pH of the brine (*s.l.*), meaning that it was acquired at room temperature. The experiment was performed for two formation waters (Ekofisk formation water (EFW) Valhall formation water (VFW)) and one produced water. It is relevant to mention that formation water sample have synthetic origin and the produced water is an offshore sample from the Halfdan field.

From the analysis of the Figure 4.1 one can verify that when Danchalk interacts with EFW at room temperature, the EFW pH has an oscillatory variation, after 24 hours of exposure to the rock sample there is a slight increase in pH, which remains stable until ca.13 days, after which it decreases. At the 16th day, one can see an rising tendency, with its higher

pH achieved after 20 days ($\text{pH} = 7.19$). followed by another slight decrease. At 70°C , the exhibited trend is opposite to the one described for room temperature with exception to the last 10 days in which both temperature conditions had shown the exact same pattern.

Regarding the VFW pH variation, one can see that both at room temperature and 70°C there is generic increase trend in pH until ca. 10 days, after which the VFW pH slightly reduces. An exception to the previous, is observed for the period after 24 hours of interaction at room temperature as it possible to see a trivial decrease in pH.

The chemical interaction of Danchalk with Halfdan produced water (HPW) in Figure 4.1 essentially depicts the pH variation at room temperature. It was not possible to measure the pH after 24 hours at 70°C due to a defect in the autoclave bottle which led to partial evaporation of the produced water, this way altering the conditions initially established for the experiment. The VFW pH has shown an increasing trend until 10 days, after which the pH has kept a constant value around 7.5.

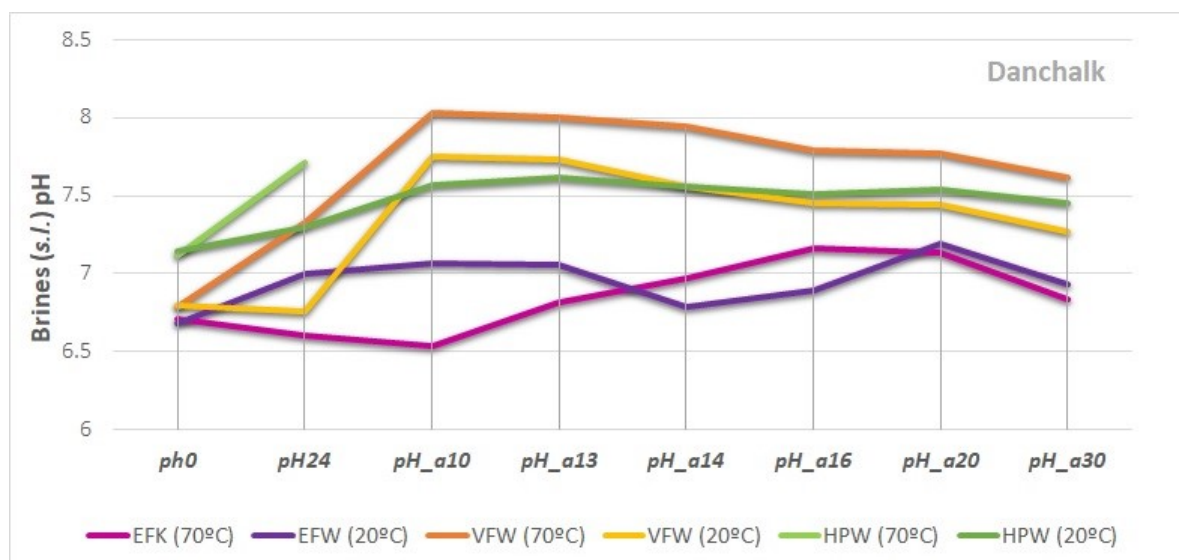


Figure 4.1: Danchalk pH variation upon interaction with Ekofisk formation water, Valhall formation water and Halfdan produced water at temperatures of 20°C and 70°C .

The integrated analysis of Figure 4.1, seems to reveal a relatively smaller capacity of VFW to dissolve the rock sample, as indicated by the higher pH values. Such behaviour is even more accentuated after 10 days of exposure. The same is observed for HPW, in a smaller extent. The experimental observations demonstrate that at higher temperature, there is a decrease in CaCO_3 solubility, meaning that calcite will precipitate and the pH will

increase. The observed behavior confirms the previously observed by other authors [27, 41]. However, and contrarily to what was expected EFW has shown the reverse tendency for the initial 13days of experiment. Such peculiarity has not been fully understood.

4.1.2 Coreflooding Experiments

The coreflooding experiments were performed for the Austin chalk core sample, at a constant temperature of 70°C and constant flow rate of 1ml/min. The core samples were saturated either with Ekofisk or Valhall formation water prior to the flooding with produced water. During the experiment the injection and outlet pressures were registered and the differential pressure (dP) calculated. Similarly the back pressure and annulus pressure were also recorded. An average of 64 measurements were recorded per minute. For the coreflooding in which the core sample had been saturated with Ekofisk formation water the code CF2 was attributed. In case of Valhall formation Water saturation the designation CF3 had been used. It must be mentioned that all the results present in current section reflect the measurements acquired until the cylinder of pump B has been emptied; due to a system malfunction it was not possible to use pump A to continue the experiments.

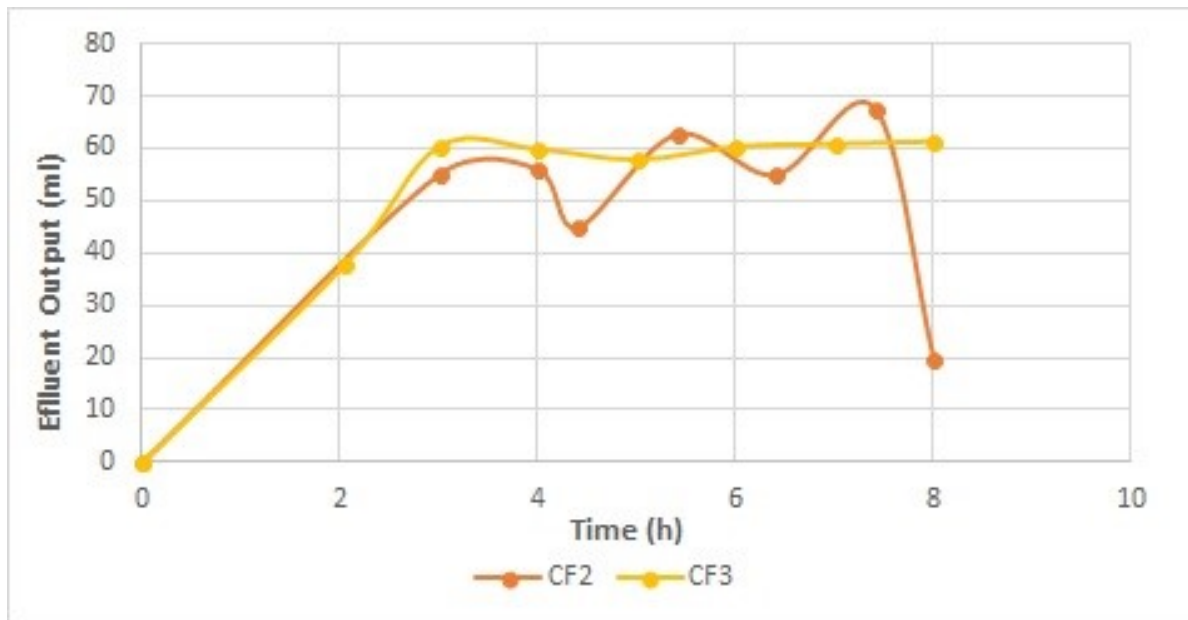


Figure 4.2: Austin Chalk coreflooding output flow-rate.

The Figure 4.2 illustrates the estimation of effluent output flow rate for the performed experiments. One has verified that in order to obtain the first effluent sample ca. 1-2

hours from the start of the experiment are required. The first effluent was obtained quicker in CF3 compared to CF2. Moreover, the output flow-rate was approximately constant around 60 ml per hour. It is relevant to mention that the low effluent collected for the last CF2 sample (ca. 20 ml) doesn't represent any variation in the core, but rather the stop of the experiment.

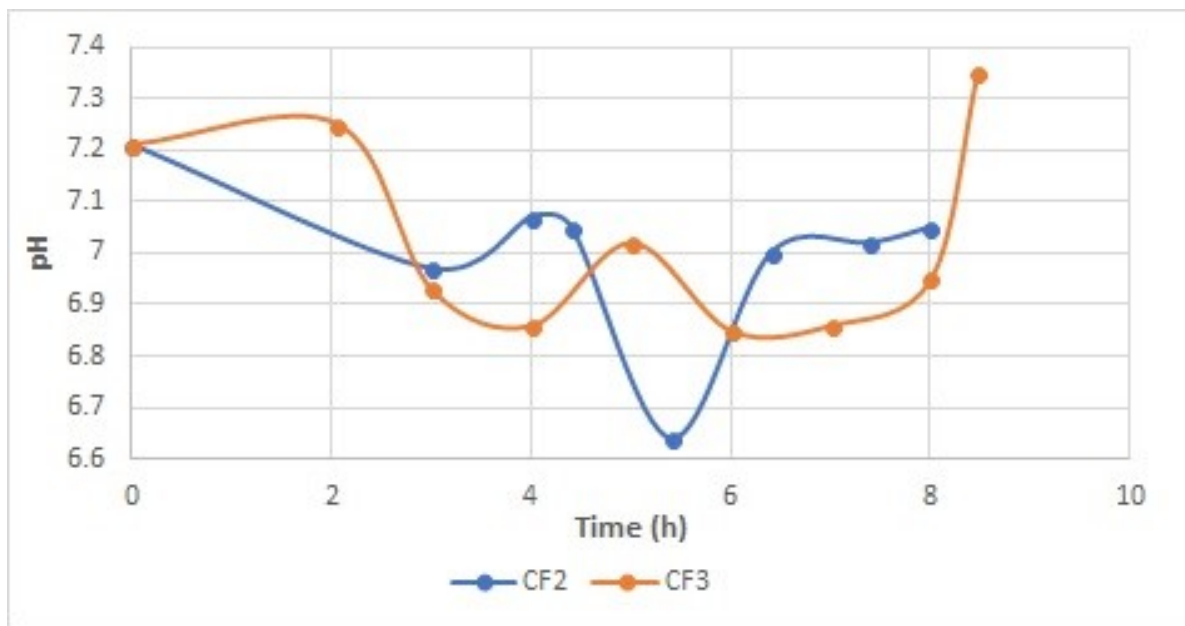


Figure 4.3: Austin Chalk coreflooding effluent pH variation over time.

The coreflooding effluent pH variation can be seen in Figure 4.3. From the analysis of the graph one can see that as general trend the effluent pH decreased over time. As main features one can denote: the sudden pH decrease followed by increase in CF2 registered after around 5 hours and 30 minutes from the start of the experiment; and the increase in pH started after ca. 7 hours in CF3. These variations can be considered as indications of dissolution and precipitation processes, that require further confirmation and cross-check to be considered evidences.

CF2: Austin chalk sample (AC3) flooding

The measurements registered for the coreflooding of the saturated Austin chalk with Ekofisk formation water are presented in the Figures 4.4 to 4.8. Figure 4.4 shows the non-clean data acquired for the differential pressure (dP) variation over time. From the

analysis of this plot it can be observed that initially the dP was approximately zero, meaning that the injection pressure was equal to the outlet pressure. In CF2 this pattern was register from 08:42 until ca. 10:16 and also from ca. 16:47 until the end of the experiment. This last event occurs after a sudden decrease in dP, which related to the emptying and refill of the pump B cylinder and attempt to continue the measurements. As can be seen from the plot it is not possible to draw any conclusions based on the data acquired after the pump cylinder is empty if the second pump is not ready to immediately take over and keep the injection flow-rate constant during the entire experimental time.

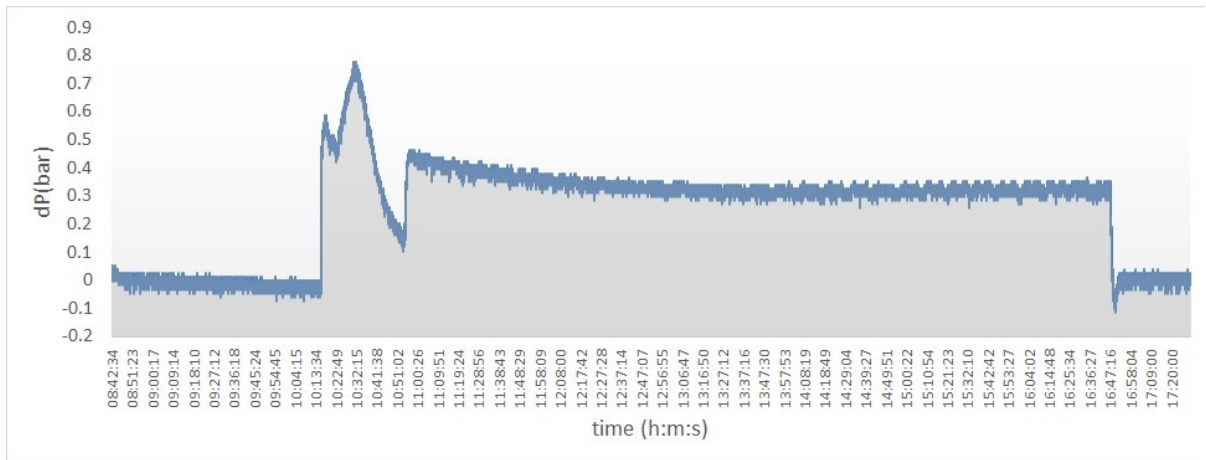


Figure 4.4: Raw data for CF2 differential pressure variation (bar) over time.

In order to overcome this technical problem, it was decided to exclude from further calculations the data concerned in the above-mentioned ranges. From this decision yields the plotted data present in Figure 4.5.

The Figure 4.6 illustrates the annulus pressure oscillation during the CF2 experimental period. It was noticed that there was a tendency for the annulus pressure to build up quickly, which led to forced a continuous adjustment of this value. The annulus pressure bleeding was done manually, by carefully regulating a gate valve attempting to reach a stable value. From the comparison of the Figures 4.5 and 4.6 it can be seen that the instability of the annulus pressure at the initial experimental hours has not influenced the variation the dP, see for example that an annulus pressure drop of 15 bar around 11:44 (Figure 4.6) doesn't reflect any change in dP (Figure 4.5) for the same hour period. However, it would be recommendable to replace the manual-operated valve for an automated device connected to a pressure traducer, this way allowing the possibility of having longer experimental periods.

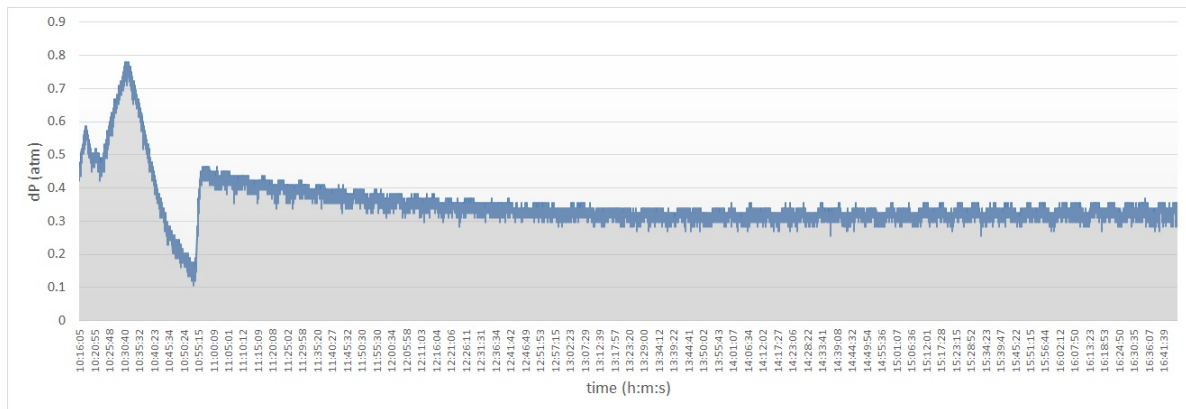


Figure 4.5: CF2 differential pressure variation (atm) over time used for permeability calculation.

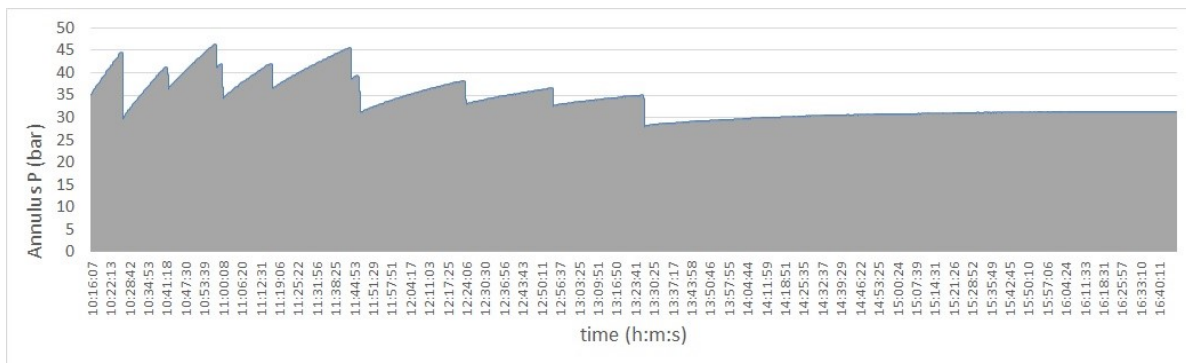


Figure 4.6: Annulus Pressure variation (bar) over time during CF2 coreflooding.

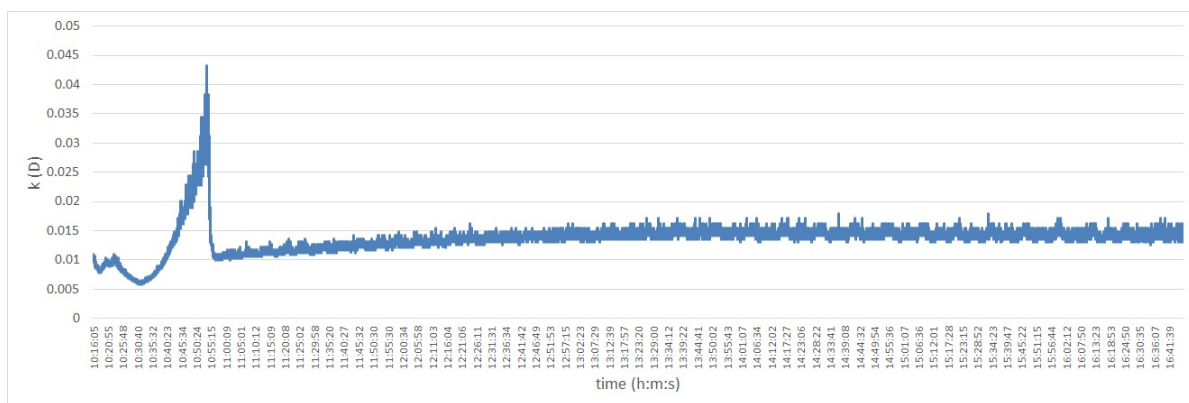


Figure 4.7: Ekofisk FW saturated Austin Chalk permeability variation (D) over time upon coreflooding with HPW at constant flow-rate (1ml/min) and constant T of 70°C.

The considerations regarding the annulus pressure stability are of major importance, since one should understand if the oscillation in dP from Figure 4.5 is a reflection of some phenomena occurring inside the core sample or a consequence linked to any other external factor.

The core sample permeability variation over time was calculated from the dP variation shown in Figure 4.5. The initial permeability and porosity of the AC3 core sample measured by the AP608 permeameter-porosimeter is presented in Table 4.1.

The permeability variation results for the Austin chalk core sample (AC3) saturated with Ekofisk formation Water and flooded with Halfdan produced water are presented in Figure 4.7. The permeability was calculated using the darcy's law (equation 3.1.1, chapter 3), assuming that dynamic viscosity (μ) of produced water at 70°C is equal to the fresh water. The dynamic viscosity of fresh water at 70°C is approximately 0.4035 cP (see Figure 3.4, chapter 3). The measurements of AC3 core sample permeability and porosity after flooding are presented in Table 4.2.

Table 4.1: Porosity and permeability of the AC3 core sample of Austin Chalk before Ekofisk formation water saturation and coreflooding. Results from AP-608 automated permeameter-porosimeter.

<i>Core Sample</i>	<i>P conf. (psi)</i>	<i>Porosity (%)</i>	<i>K air (D)</i>	<i>K Klinkenberg (D)</i>
AC3	530.90	28.98	0.031	0.030
AC3	625.40	28.91	0.031	0.030
AC3	749.10	28.89	0.031	0.030
AC3	869.00	28.84	0.031	0.030
AC3	977.70	28.82	0.031	0.030

Table 4.2: Porosity and permeability of the AC3 core sample after coreflooding. Results from AP-608 automated permeameter-porosimeter.

<i>Core Sample</i>	<i>P conf. (psi)</i>	<i>Porosity (%)</i>	<i>K air (D)</i>	<i>K Klinkenberg (D)</i>
AC3	527.50	27.70	0.024	0.022
AC3	750.90	27.64	0.024	0.023
AC3	982.70	27.60	0.024	0.023

From the analysis of the Figure 4.7 it is possible to verify that the main changes in

permeability occur in the time range 10:16 to 10:55. The permeability initially oscillates around 0.01 D, decreasing to ca. 0.005 (see time = 10:23). Later on, around 10:30 the permeability starts progressively increasing reaching a maximum value of ca. 0.044 D at 10:55. The permeability decrease is thought to be associated to the deposition of mineral scale and blockage of flow-path. The recover and increase of permeability is justified by the finding of a new flow-path. The quick permeability increase most probably correspond to the existence of easy paths or mineral dissolution.

Following the maximum permeability reached, it was registered a sudden decrease in permeability to a value of 0.01 D. This pattern is followed by a slow recover of the permeability which reaches a stable value around 0.015 D. This value is considered the final permeability of the core.

The previously mentioned sudden permeability reduction is thought to be a "false decrease", meaning that one think it doesn't correspond to any mineral deposition, but is rather an artifact as its time frame matches the exact start of the effluent outcome.

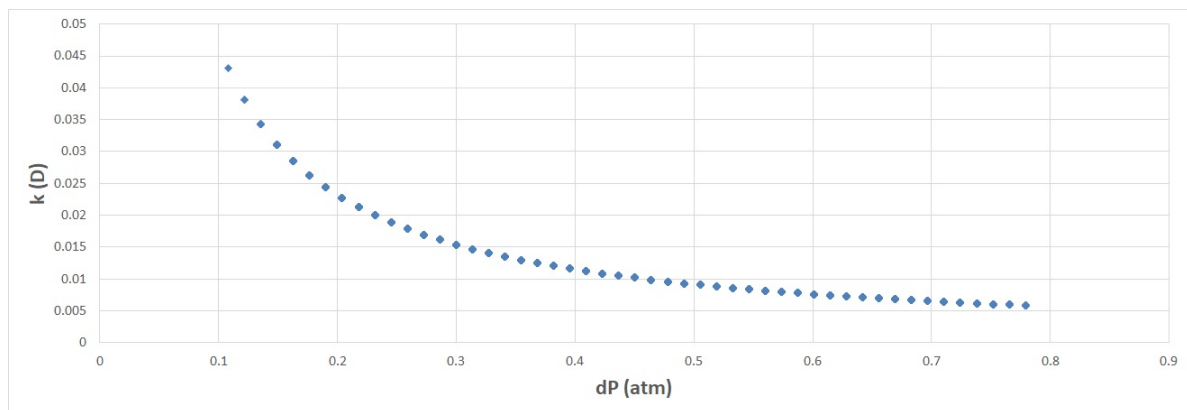


Figure 4.8: Permeability (D) *versus* differential pressure (atm) for Austin Chalk AC3 sample saturated with Ekofisk formation water and flooded with Halfdan produced water.

The results provided in Tables 4.1 and 4.2, show that overall there was a permeability decrease of 0.007 D (or 0.016 D if one compares the values from Figure 4.7 to the Table 4.2) and porosity reduction of 1.3% in average if comparison is made from the values obtained prior and after the core saturation and flooding. Such evidence is compatible with the increase in the measured weights (meaning more mass has been added) for the core at the various stages, *i.e.*, dry core, saturated core and flooded core, see Tables 3.8

and 3.9 in Chapter 3. Moreover, the final permeability value estimated from the Figure 4.7 is far from the 0.024 D air permeability measured by the AP608 (see Table 4.2).

The Figure 4.8 illustrates the existing relation of the differential pressure and permeability. As would be expected the decline in permeability values relates to an increase in the dP, and it is required higher injection pressure to achieve the same permeability.

CF3: Austin chalk sample (AC4) flooding

The CF3 coreflooding was performed for the Austin chalk core sample reference as AC4, which was initially saturated with Valhall brine and later on flooded with Halfdan produced water.

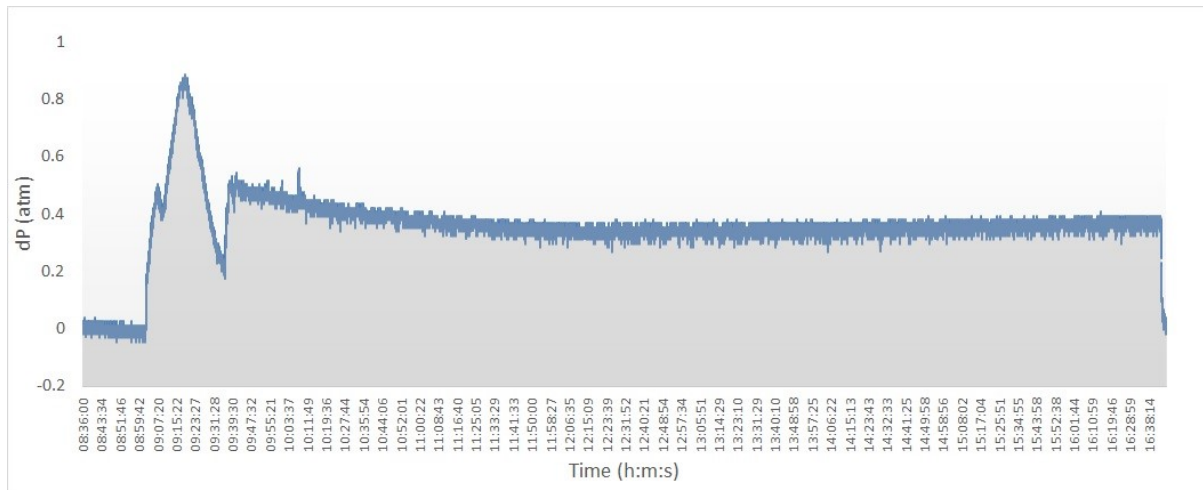


Figure 4.9: Raw data for CF3 differential pressure variation (atm) over time.

Figure 4.9 represents the raw data acquired for the differential pressure variation over time. Similarly to what has been described for CF2, initially the dP oscillated around the 0 atm, which is related to an equal value for the inlet and outlet pressures. This pattern was registered until ca. 09:01, after which there was a double step increase in the differential pressure: at first the dP increased until ca. 0.5 atm, then decreased to 0.4 atm and increased again reaching a maximum ca. 0.9 atm. After the maximum dP is achieved, it was registered a step decrease in dP until 0.2 atm, which is then followed by an increase in dP up to ca. 0.5 atm. After this, the dP slightly decreased and remained stable around 0.4 atm. As previously mentioned for CF2, the sudden differential pressure decrease

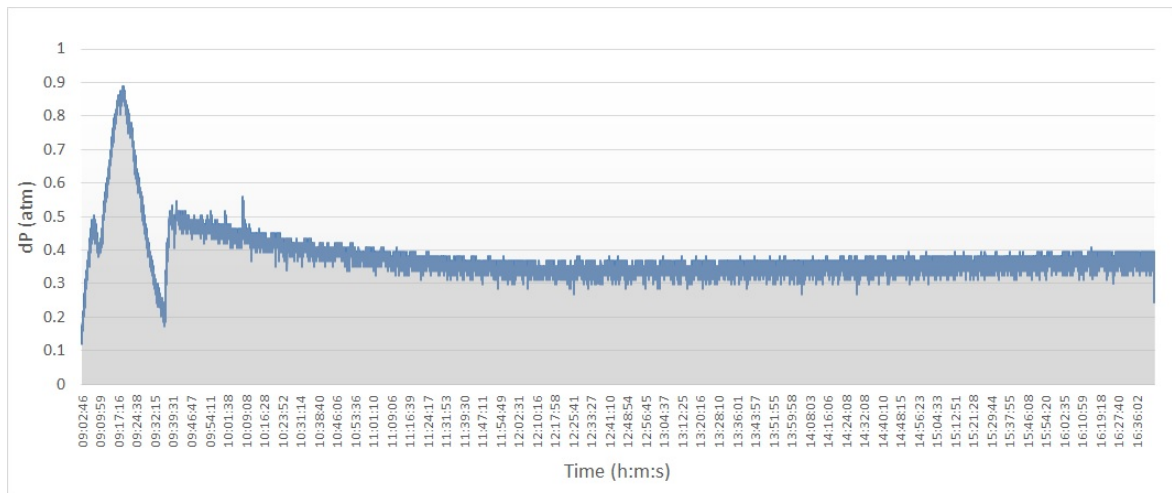


Figure 4.10: CF3 differential pressure variation (atm) over time used for permeability calculation.

around approximately 09:30 is thought to be linked to the start of effluent outcome, as once again there is a precise match for the time-frame in which this phenomenon occurs.

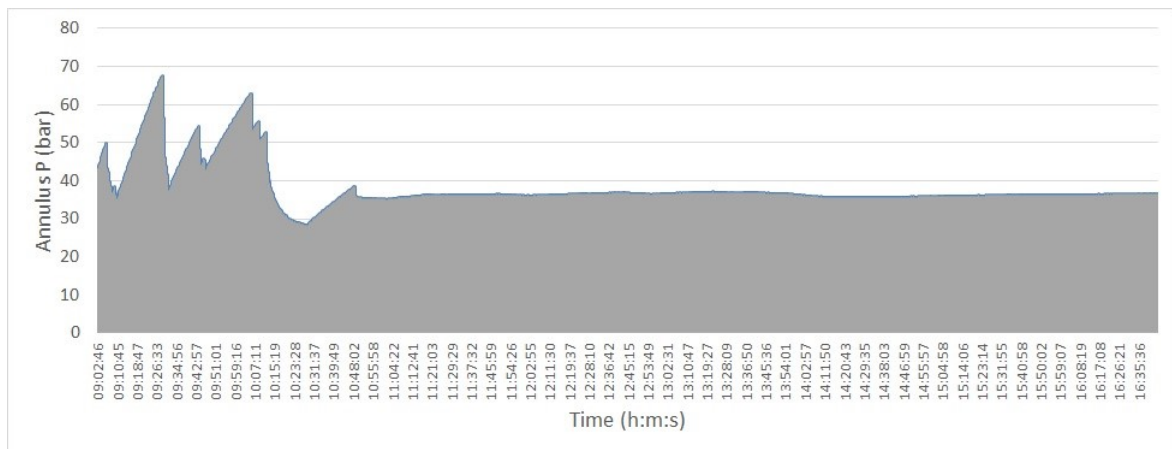


Figure 4.11: Annulus Pressure variation (bar) over time during CF3 coreflooding.

The steep dP decrease observed at the end of the experiment is once more linked to the emptying of the pump cylinder and end of the experiment.

The figure 4.10 illustrates the "clean" differential pressure data taken for permeability calculations. The Figure 4.11 shows the annulus pressure variation over time for the CF3 coreflooding experiment. As above-mentioned the initial instability of this parameter does not influence the acquired dP data, see for example 20 bar pressure drop occurred from

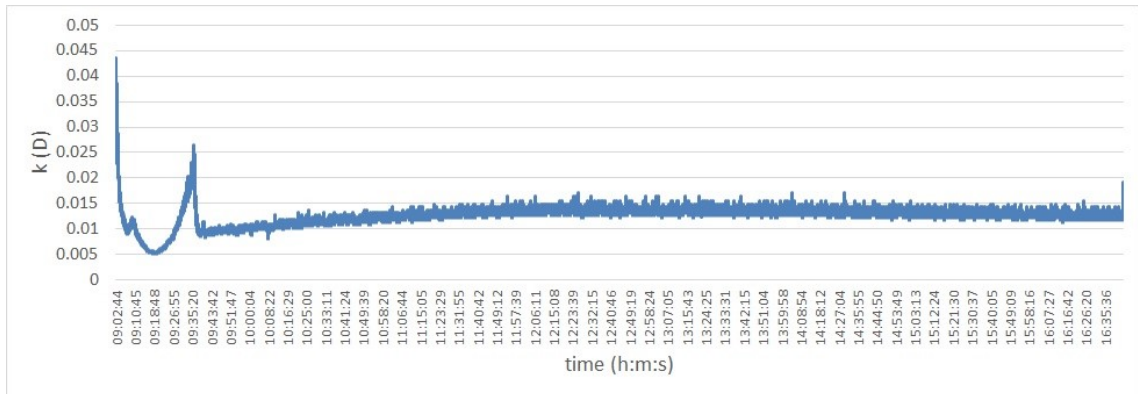


Figure 4.12: Valhall FW saturated Austin Chalk AC4 sample permeability variation (D) over time upon coreflooding with HPW at constant flow-rate (1ml/min) and constant T of 70°C.

ca. 10:15 until ca. 10:25 (Figure 4.11) corresponds to a constant dP (Figure 4.10).

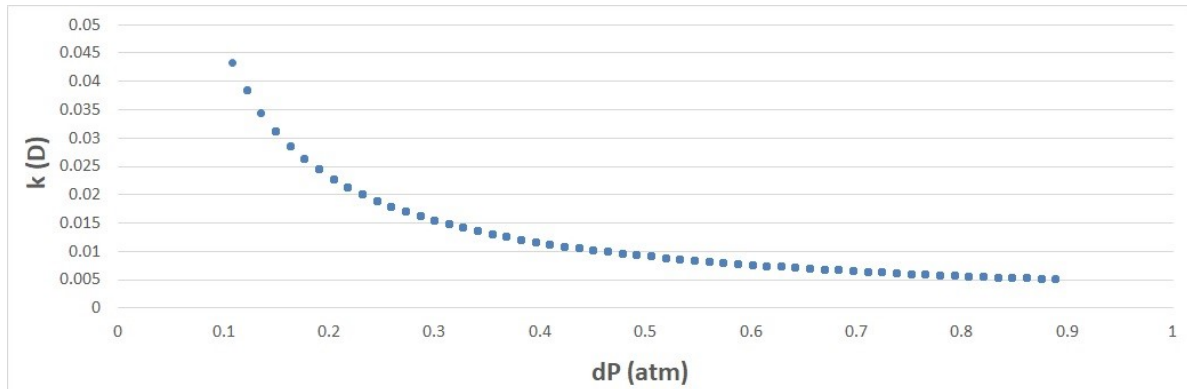


Figure 4.13: Permeability (D) *versus* differential pressure (atm) for Austin Chalk saturated with Valhall formation water and flooded with Halfdan produced water.

The Figure 4.12 depicts the permeability change over time, for the Austin chalk core sample AC4 after Valhall brine saturation and flooding with Halfdan produced water.

The permeability was calculated by applying the darcy's law (see equation 3.1.1) to the dP shown in Figure 4.10. From the interpretation of the pattern exhibited in Figure 4.12, one can see that the permeability is relatively high at the beginning (ca. 0.045 D) of the coreflooding. This value is the maximum permeability registered for the AC4 core sample and is followed by a step decrease in the permeability curve, reaching approximately 0.005 D in less than one hour from the starting time of the experiment. Such behavior exhibited by the permeability curve is once again attributed to mineral precipitation with flow path

obstruction. At ca. 9.10 is registered a small permeability increase which can reflect one of two possibilities: a) localized mineral dissolution, which temporary eases the fluid flow; b) change in the fluid-flow path after flow blockage.

Contrarily to what has been described and similarly to what has been seen CF2, the permeability decline verified at approximately 09:35 corresponds to the start of the effluent outcome, meaning that this result is a "false" reduction in permeability. After ca. 09:43 the permeability has been slowly reestablished to a constant value of ca. 0.013 D.

The Table 4.3 presents the gathered porosity and permeability measurements for the core sample prior to the saturation and flooding experiments. If one compares the permeability value obtain from Figure 4.12 to the initial value mentioned in Table 4.3 it is possible to say that there was a permeability reduction of approximately 0.017 D. Once again, this is consistent with the mass increment verified for the core sample (see Tables 3.8 and 3.9, chapter 3). The Figure 4.13 depicts the same trend shown in Figure 4.8.

Table 4.3: Porosity and permeability of the AC4 core sample of Austin Chalk before valhall saturation and coreflooding. Results from AP-608 automated permeameter-porosimeter.

<i>Core Sample</i>	<i>P conf. (psi)</i>	<i>Porosity (%)</i>	<i>K air (D)</i>	<i>K Klinkenberg (D)</i>
AC4	475.20	28.27	0.029	0.028
AC4	620.40	28.23	0.030	0.028
AC4	745.90	28.18	0.030	0.028
AC4	861.90	28.16	0.030	0.028
AC4	997.60	28.12	0.030	0.028

4.1.3 Ionic Compositions: results from ICP-OES, IC and TC

The chemical variations regarding the ionic concentration of the effluent samples of the coreflooding experiments were investigated by the help of several analytical methods, namely, inductively coupled plasma - optical emission spectrometry, ion chromatography and total carbon.

Figures 4.14 to 4.16 depict the brines (*s.l.*) ionic concentration variation acquired by ICP-OES and IC. All results were normalized for the seawater composition, which was taken

from the literature [23]. In order to ease the reading and facilitate the writing the ionic charges of each ion will be omitted in the following paragraphs and plots.

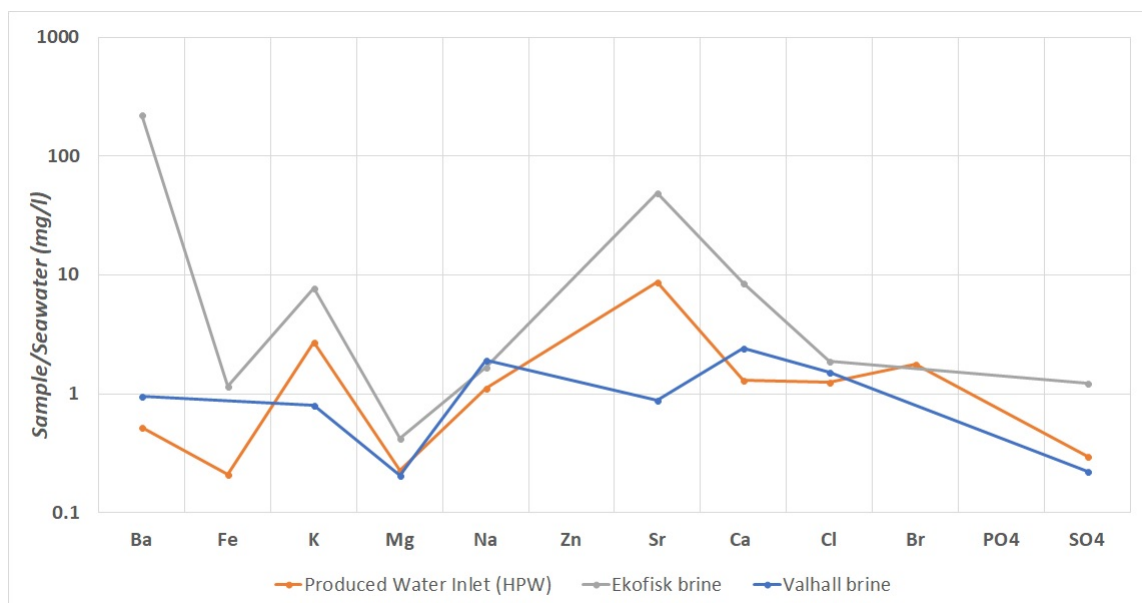


Figure 4.14: Cationic concentrations of Halfdan produced water (inlet), Ekofisk and Valhall formation waters normalized to seawater composition. For display purposes, Ba concentrations of 0 mg/l have been increased to 0.05 mg/l.

From the analysis of the Figure 4.14 one can verify that Ekofisk brine (EFW) shows a relatively enriched pattern comparing both to the seawater (SW) and produced water (HPW) or Valhall brine (VFW). This is valid for the majority of the metals, being particularly evident for *Ba*, *K*, and *Sr*. Exception has to be made for the *Mg* which is relatively less concentrated in all plotted brines (*s.l.*) comparing to the seawater. Additionally, it is possible to observe that the Halfdan produced water, although less concentrated, is characterized by the same pattern presented for the Ekofisk brine with exception for the *Br*.

The Figure 4.15 illustrates the ionic composition variation for 3 effluent samples of the coreflooding CF2. PW1A corresponds to the ionic composition obtained for the sample collected at the first hour since the start of the effluent output; PW4A represents the fourth collected sample after approximately four hours; and PW7A was sampled after ca. seven hours from the start of the effluent output.

The analysis of the Figure 4.15 one can see the effluent samples are relatively enriched in *Ba*, *Fe*, *K* (exception for PW4A), *Ca*, *PO₄* compared to the Halfdan produced water. This trend should also be compared to the values present for the Ekofisk brine, once one

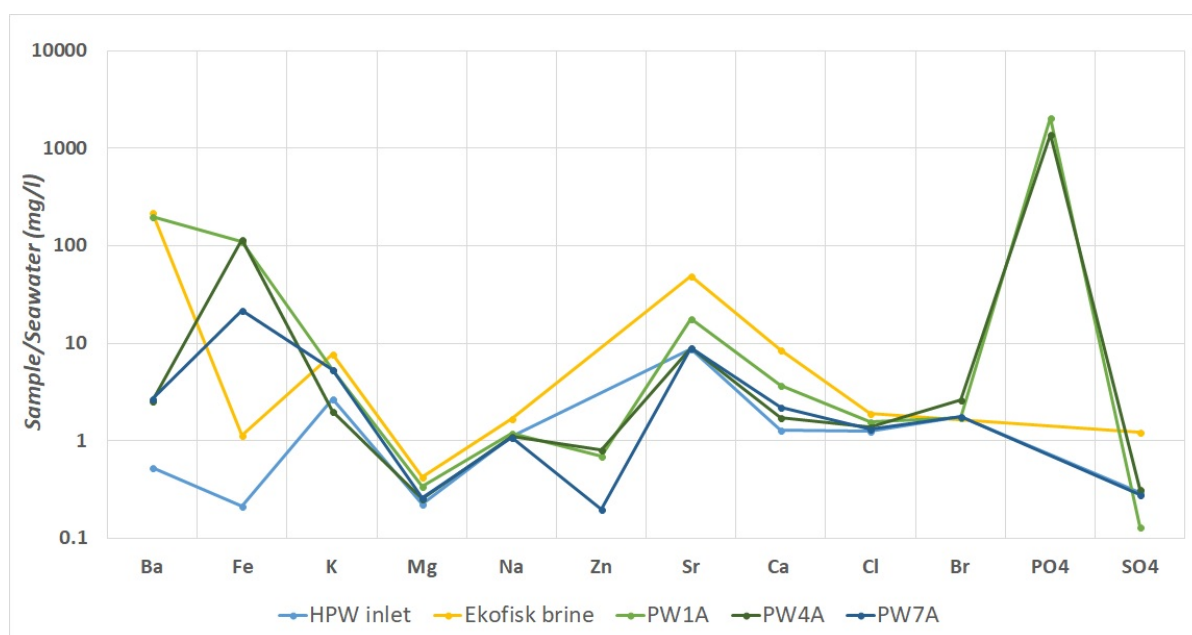


Figure 4.15: Ionic concentrations of produced water (inlet), Ekofisk and produced water effluents normalized to seawater composition. For display purposes, Ba concentrations of 0 mg/l have been increased to 0.05 mg/l.

is interested in identifying possible mineral precipitation or dissolution. Apart from the effluents enrichment in Fe and PO_4 , the variations in concentration are of low magnitude order. The PO_4 enriched pattern (over 1000 mg/l) can be explained by one of the two possibilities: a) contamination coming from the DI water used to prepare the synthetic Ekofisk brine; b) incorporation of phosphate due to dissolution of organic or inorganic phosphate from the core sample. The most probable hypothesis seems to be the second, in which phosphate dissolution has occurred, once the measurements performed for EFW and HPW have not detected presence of phosphate. Regarding the Fe concentrations these are thought to be contamination original from minor rust in the coreflooding piston. The relative K depletion exhibited by PW4A its thought to be related to a localized precipitation of a K-bearing mineral. It was also noticed SO_4 depletion in the effluent outcome PW1A, which might represent a mineral deposition with consequent retention in the core sample, once there is availability of various divalent cations. Since the temperature at which this study was carried out is $70^\circ C$, the Ba abundance is relatively high (see Ba concentration, Table 4.4) and the $BaSO_4$ solubility is very low (see Figure 2.4, Chapter 2), it is suspected that barite precipitation has occurred.

The Figure 4.16 depicts the ionic concentration variation for the Austin chalk AC4 core

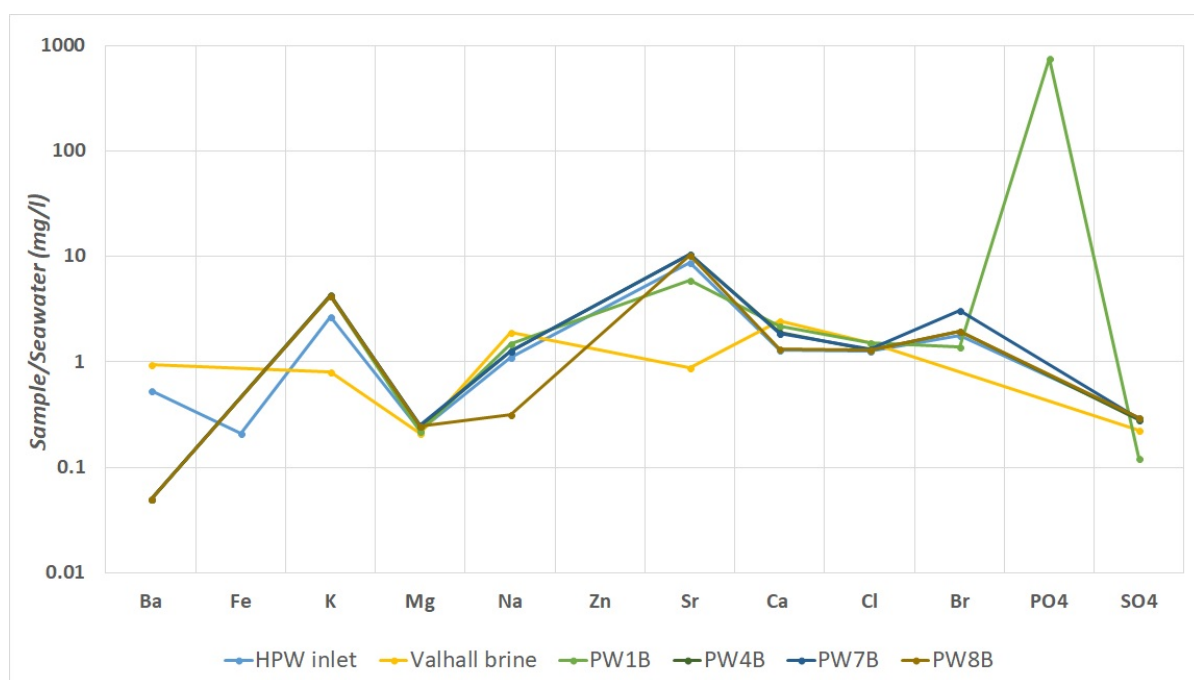


Figure 4.16: Ionic concentrations of produced water (inlet), Valhall and produced water effluents normalized to seawater composition. For display purposes, Ba concentrations of 0 mg/l have been increased to 0.05 mg/l.

sample, which was subjected to Valhall brine saturation followed by HPW flooding (CF3). From the analysis of the plot one can verify that there is notorious relative depletion of *Ba* in all effluents, meaning that it has been retained in the core sample. PW8B is also characterized by a prominent relative reduction in *Na* concentration. Also there is a slight relative depletion of *Ca* (exception for PW1B). These ionic relative depletions are thought to be related to mineral scale deposition. Similarly to what was described for the CF2 coreflooding, the *K* concentration is relatively high for all the effluent samples. Moreover, the PW1B is also characterized by an enrichment in phosphate anion, which is thought to come from the sample dissolution, possibly biogenic phosphate, from organisms shells.

The Figures 4.17 and 4.18 illustrate the organic and inorganic carbon content of HPW and its effluents, respectively. Three effluent samples were analyzed for CF2 and four effluent sample for CF3. Regarding the organic carbon concentration (Figure 4.17) one can see that there is a relative decrease in organic carbon content for the first effluent sample (PW1) in both coreflooding experiments, which is followed by an increase in upcoming effluents. Such pattern is more evident in CF2.

The oil in water content (OIW) was measured by GC-FID for the Halfdan produced water and a concentration of 63.82 ppm was obtained. This value is higher than the maximum allowed value for produced water discharge defined by OSPAR regulation, which is 30 ppm. If discharge is to be considered, further treatments should be applied in order to decrease the dispersed oil concentration, which would imply investment from the company. The Figure 4.18 concerns the total inorganic carbon (mg/l) present in the produced water and its effluents. From the graph, it can be observed that CF3 effluent were progressively more depleted in inorganic carbon over time, reaching a constant value at ca. 35mg/l. This behaviour trend seems to indicate partial precipitation and retention of the carbonate and bicarbonate ions in the core sample. The gathered results for CF2 reveal that, as generic trend, the inorganic carbon tends to decrease over time. However, such pattern does not show a continuous decrease, since PW4A registered slightly higher concentration comparing to PW1A.

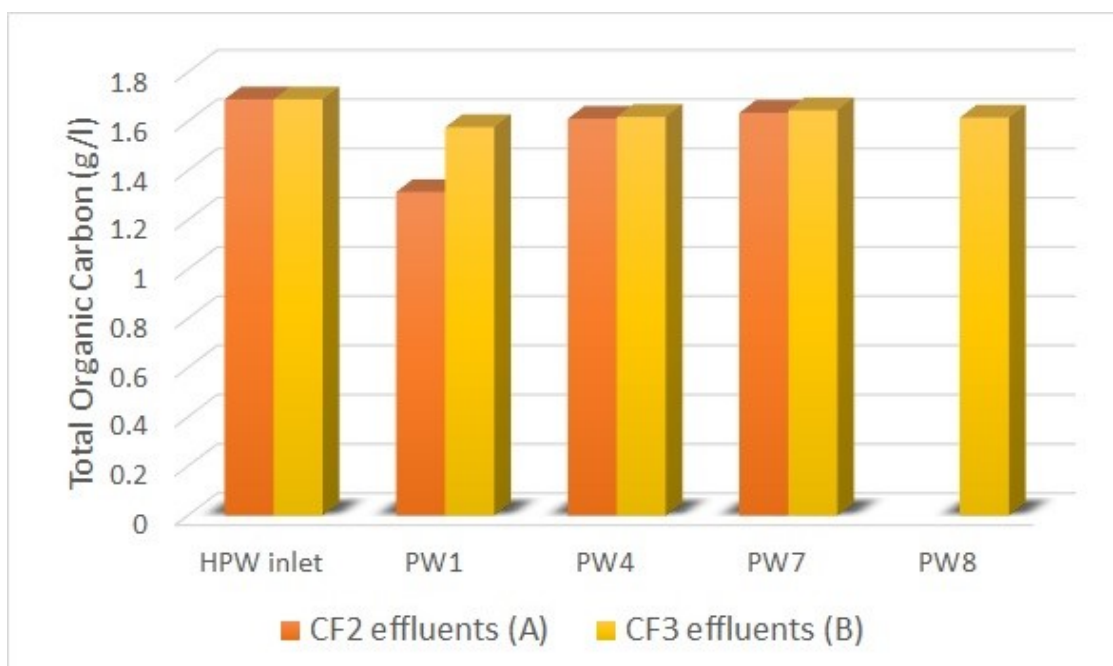


Figure 4.17: Total organic carbon content of Halfdan produced water prior to injection and in coreflooding effluents. Results acquired by Analytik jena multi N/C 2100 analyzer.

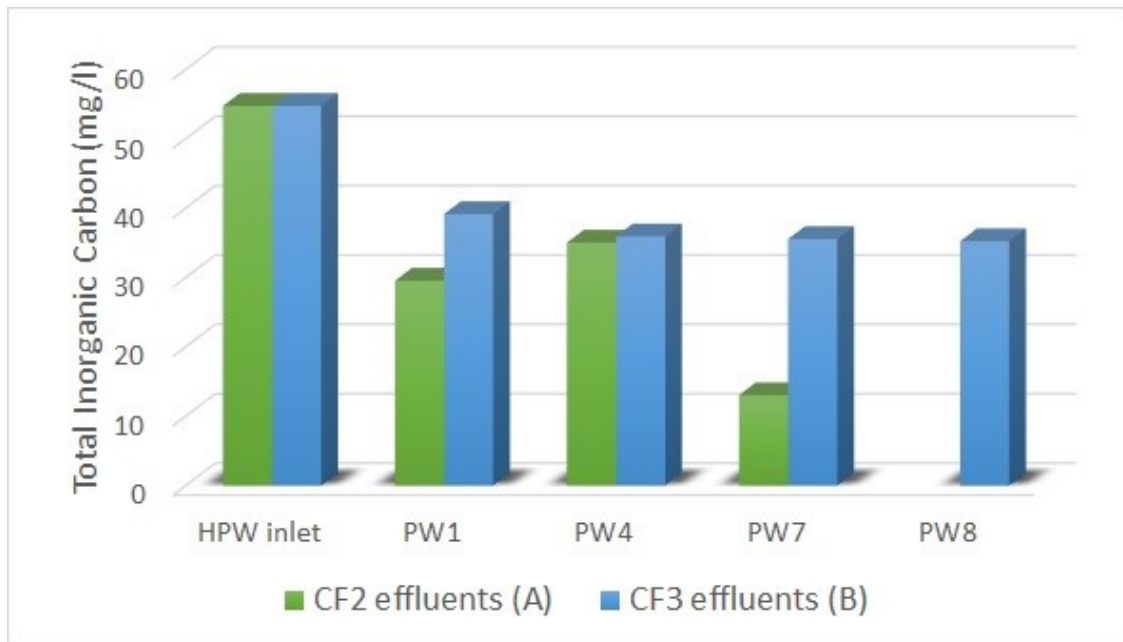


Figure 4.18: Total inorganic carbon content of Halfdan produced water prior to injection and in coreflooding effluents. Results acquired by Analytik jena multi N/C 2100 analyzer.

4.1.4 Final Remarks

The gathered results and integrated analysis have demonstrated a porosity and permeability reduction linked to the Austin chalk saturation with Ekofisk and Valhall brines and posterior flood with Halfan produced water at a temperature of 70°C.

The permeability reduction estimation for CF2 and CF3 is 0.016 D and 0.017 D, respectively. The results similarity was not expected to occur. The author was anticipating to see a relatively higher permeability reduction associated to the coreflooding performed for the core saturated with Ekofisk, since this brine is characterized by higher ionic strength (and so higher TDS) compared to the Valhall brine (see Table 4.4). However, for the current experimental conditions the previously described has not been observed. It is relevant to mention that all obtained results constitute only indications and can not be taken as certain to occur, if not tested for the well pressure and temperature variation profiles. Ideally, such experiment should be performed for lower flow-rates and bigger exposure times which will enable the chemical reaction to happen. Even-though, in the time-frame available it was possible to verify what is thought to be slight barite precipitation, potassium, carbonate and bicarbonate ions retention and localized phosphate dissolution. Moreover,

although all registered experimental variations in terms of dP and K are very small, they have been consistent to what was indicated by other analytical methods used.

Table 4.4: Ionic composition (ppm), ionic strength (mol/l), density (g/cm^3) and pH presented by Ekofisk brine (EFW), Valhall brine (VFW) and Halfdan produced water (HPW).

Brine (s.l.)	Na (ppm)	Cl (ppm)	K (ppm)	Mg (ppm)	Ca (ppm)	Fe (ppm)	Ba (ppm)	Sr (ppm)	Br (ppm)	SO ₄ (ppm)	HCO ₃ (ppm)	Ionic strength (mol/l)	Density @23°C (g/cm ³)	pH @23°C
EFW	50.2636	40.1497	0.1883	0.9004	2.4931	0.0000	0.0134	0.0972	0.0000	0.0000	0.0648	1.5594	1.0536	6.40
VFW	43.3215	30.0299	0.1201	0.3237	0.7298	0.0000	0.0000	0.0000	0.0000	0.0073	0.1463	1.1127	1.0401	7.30
HPW	22.2312	19.0513	0.6711	0.4840	0.3220	0.0001	0.0000	0.0147	0.0180	0.0850	0.0147	0.6758	1.0334	7.21

5 Conclusions

The current report presented the gathered results concerning the scale potential associated to produced water injection. Chalk samples from two different provenances were used to understand the mineral scale deposition or dissolution if produced water was brought into contact with high salinity brines. In total, two coreflooding experiments were carried out for constant flow-rate of 1ml/min and constant temperature 70°C. The ionic compositions for the brines, injection produced water and produced water effluents were measured by ICP-OES, IC, TC and the ionic strength calculated.

Initially, it was thought to simulate of scale formation using phreeqc software, however due to technical problems external to the author, which led to the postpone of the experimental works it was not possible to carry out the intended simulation.

Scale deposition poses one of major threats in oil industry. As previously mentioned, the scale precipitation from injected water is able to smother a well within a 24-hour period if not correctly controlled. Therefore, prior to produced water re-injection there is the need of an in-depth study of the scale potential. The results obtained from the current study serve as indications, which must be further confirmed by numerical simulations at the reservoir pressure and temperature.

Summarizing, the main conclusions of this master thesis are as follows:

1. The valhall brine presents a relatively smaller capacity to dissolve the Danchalk rock sample, as indicated by the higher pH values for the beaker test;
2. The Beaker test experimental observations have demonstrated that at higher temperature, there is a decrease in $CaCO_3$ solubility, meaning that calcite will precipitate and the pH will increase;
3. The pH variations can be considered as indications of dissolution and precipitation processes, as it was possible to verify the consistent indications from the effluent ionic composition analysis;

4. The initial annulus pressure oscillation does not influence the differential pressure, and consequently does not induce to false evidences regarding the permeability measurements;
5. The saturation of the Austin chalk sample with Ekofisk brine followed by Halfdan produced water flooding led to a porosity reduction of 1.3% and permeability reduction of 0.016 D;
6. The saturation of the Austin chalk sample with Valhall brine a subsequent flood with Halfdan produced water caused permeability reduction of 0.017 D. The porosity is estimated to be reduced but the numerical value as not possible to obtain, due to equipment malfunction;
7. The decline in permeability values relates to an increase in the dP, and it is required higher injection pressure to achieve the same permeability;
8. All obtained results constitute indications and can not be taken as certain to occur, before further testing for the well pressure and temperature variation profiles;
9. For the conditions used in CF2, there is a possibility of barite precipitation and deposition of a potassium bearing mineral. Also, indications have been found for phosphate dissolution;
10. For the conditions used in CF3, *Ba*, *Ca* and *Na* mineral scale is possible to occur, as there is evidence for the retention of these metals in the core sample. Once again, indications have been found for phosphate dissolution;
11. CF3 effluent showed progressive depletion in inorganic carbon over time, reaching a constant value at ca. 35 mg/l after approximately 4 hours. Such pattern is compatible to the occurrence of partial precipitation and retention of the carbonate and bicarbonate ions in the core sample; Same behavior is observed for CF2, although not this last has not been a continuous process;
12. The oil in water value measured for Halfdan produced water is 63.82 ppm, which is above the maximum allowed for water discharge following the OSPAR regulation;

5.1 Future Work

The mineral scale investigation is of major importance, since its prevention and correct treatment can prevent hazards, reduce costs and turn the production more efficient. As future work recommendations there are various possibilities that would be of interest, such as:

1. Test different flow-rates, keeping all the other experimental variables constant;
2. Test a range of temperatures, while keeping constant the flow-rate, the brine saturation selection and the produced water flooding;
3. Select experimental condition that provided the highest porosity and permeability reduction, and the damaged core and repeat the coreflooding this time adding a scale inhibitor adequate to the mineral scale suspected to be formed. Compare the results;
4. Perform the beaker test variation B and compare the results;
5. Saturate the produced water with CO_2 and repeat the experimental tests.

Bibliography

- [1] T. M. Aabø. Background study of the kraka, dan and halfdan fields. 61 pp, 2006.
- [2] AGA. Gas chromatography. flame ionization detector. http://www.aga.is/internet.lg.lg.isl/is/images/AGA%20HIQ%20Flame%20Ionization%20Detector%20Datashet%20UK648_102263.pdf?v=1.0, 2018. [Online; accessed 15-May-2018].
- [3] T. Ahmed. *Reservoir Engineering Handbook*. Gulf Professional Publishing, 2001.
- [4] A. Alabi, M. Chiesa, C. Garlisi, and G. Palmisano. Advances in anti-scale magnetic water treatment. 1:408–425pp, 2015.
- [5] A. Binmerdhah and A. Azam Mohd Yassin. Barium sulfate scale formation in oil reservoir during water injection at high-barium formation water. 7:2393–2403 pp, 12 2007.
- [6] A. Binmerdhah and A. Azam Mohd Yassin. Laboratory study and prediction of calcium sulphate at high-salinity formation water. 1:pp, 12 2008.
- [7] C. B. Boss and K. J. Fredeen. Concepts, instrumentation and techniques in inductively coupled plasma optical emission spectroscopy. Perkin Elmer, USA, 7 2004.
- [8] M. Crabtree, D. Eslinger, P. Fletcher, M. Miller, A. Johnson, and G. King. Fighting scale-removal and prevention. 11 (3):30–45pp, 1999.
- [9] M. D’Heur. Porosity and hydrocarbon distribution in the north sea chalk reservoirs. *Marine and Petroleum Geology*, 1(3):211 – 238, 1984.
- [10] E. dos Santos Godinho. Effectiveness of produced water in advanced waterflooding: estimation of the wettability alteration by modified flotation technique. unpublished 9th Semester Report, 2017.

- [11] E. dos Santos Godinho and K. Jefimov. Wettability alteration in chalk using flotation technique. unpublished 8th semester report in oil and gas production, Aalborg University, 2017.
- [12] M. Garba and M.S.Sulaiman. Oilfield scales treatment and managerial measures in the fight for sustainable production. 2:19–36pp, july 2014.
- [13] D. L. Gautier. Kimmeridgian shales total petroleum system of the north sea graben province. 2204-C:24 pp, 2005.
- [14] J. M. Guthrie and J. R. Ferguson. Overview of x-ray fluorescence, 2012.
- [15] J. M. Hancock. The petrology of the chalk. *Proceedings of the Geologists' Association*, 86(4):499–535pp, 1975.
- [16] C. E. Housecroft. *Inorganic Chemistry. Second Edition*. Pearson Education Limited, 2005.
- [17] C. S. Inc. Ap-608 automated permeameter-porosimeter. [http://www.coretest.com/CSI_Website_English/products_list\(Oil%20&%20Gas\).html](http://www.coretest.com/CSI_Website_English/products_list(Oil%20&%20Gas).html), 2018. [Online; accessed 23-May-2018].
- [18] M. ion analysis. 819 ic detector / 820 ic separation center manual. Metrohm AG, Oberdorfstrasse 68, CH-9101 Herisau, Switzerland, 7 2004. Instructions for Use 8.819.1013.
- [19] F. Jakobsen and C. Andersen. Late cretaceous basin development of the southern danish central graben. *Geological Survey of Denmark and Greenland Bulletin*, 20:15–18pp, 2010.
- [20] T. Jones, H. Henrik Kogsboll, and J. Koldig. Downhole scale management in gorm, dan, and halfdan, and implications to industry trends, 05 2006.
- [21] D. Keszthelyi, D. K. Dysthe, and B. Jamtveit. Compaction of north-sea chalk by pore-failure and pressure solution in a producing reservoir. *Frontiers in Physics*, 4:4, 2016.
- [22] T. E. Larson, A. M. Buswell, H. F. Ludwig, and W. F. Langelier. Calcium carbonate saturation index and alkalinity interpretations. *Journal of the American Water Works Association*, 34(11):1667 – 1684 pp, 1942.
- [23] LennTech. Major ion composition of seawater. <https://www.lenntech.com/composition-seawater.htm>, n.d. [Online; accessed 28-April-2018].

- [24] C. LibreText. Ionic solids, 2016.
- [25] R. Martin, J. D. Baihly, R. Malpani, G. J. Lindsay, and W. K. Atwood. Understanding production from eagle ford-austin chalk systems. SPE 145117:28 pp, 2011.
- [26] G. F. Mason B. Tomson, Amy T. Kan and M. Al-Thubaiti. Norm scale formation, control, and relation to gas hydrate control. Report from 10th Annual International Petroleum Conference, IPEC, Tulsa, 2003.
- [27] A. Merdhah. The study of scale formation in oil reservoir during water injection at high-barium and high-salinity formation water. Master’s thesis, Faculty of Chemical and Natural Resources Engineering, Universiti Teknologi Malaysia, 11 2007.
- [28] F. J. Millero, R. Feistel, D. G. Wright, and T. J. McDougall. The composition of standard seawater and the definition of the reference-composition salinity scale. *Deep Sea Research Part I: Oceanographic Research Papers*, 55(1):50 – 72, 2008.
- [29] J. Moghadasi, H. Müller-Steinhagen, M. Jamialahmadi, and A. Sharif. Model study on the kinetics of oil field formation damage due to salt precipitation from injection. *Journal of Petroleum Science and Engineering*, 43(3):201 – 217, 2004.
- [30] A. J. Ninfa, D. P. Ballou, and M. Benore. Chromatography. In *Fundamental Laboratory Approaches for Biochemistry and Biotechnology*, chapter 5. Wiley, USA, 2010.
- [31] E. Nygaard, K. Lieberkind, and P. Frykman. Sedimentology and reservoir parameters of the chalk group in the danish central graben. 62:177–190 pp, 01 1983.
- [32] J. Oddo and M. B. Tomson. Why scale forms and how to predict it. 9, 01 1994.
- [33] E. Otumudia and A. Ujile. Determining the rates for scale formation in oil wells. 6:2248–9622 pp, 09 2016.
- [34] A. Paar. Viscosity of water. <https://wiki.anton-paar.com/en/water/>, n.d. [Online; accessed 26-April-2018].
- [35] S. R. Panthi. Carbonate chemistry and calcium carbonate saturation state of rural water supply projects in nepal. In *Seventh International Water Technology Conference, Egypt*, pages 545–560 pp, 04 2003.
- [36] K. Pearson. Geologic models and evaluation of undiscovered conventional and continuous oil and gas resources—upper cretaceous austin chalk, u.s. gulf coast. 2012–5159:26 pp, 2012.

- [37] Reagecon. Certificate of gravimetric preparation–ica-dx-721. http://coa.reagecon.com/uploads/documents/ICA_DX_721_ICADX72115C1_Supplementary.pdf, 2016. [Online; accessed 15-May-2018].
- [38] M. Sohal. *Wettability modification in chalk: systematic evaluation of salinity, brine composition and temperature effects*. PhD thesis, 2016.
- [39] Preface. In J. K. Fink, editor, *Oil Field Chemicals*, page 495pp. Gulf Professional Publishing, Burlington, 2003.
- [40] R. D. Tate. Composition for removing scale, 06 1995. US Grant: US5685918A.
- [41] M. Tungesvik. The scale problem, scale control and evaluation of wireline milling for scale removal. Master’s thesis, Faculty of Science and Technology, University of Stavanger, 6 2013.
- [42] R. University. Icp-oes equipment. <https://www.ru.nl/science/gi/facilities-activities/elemental-analysis/icp-oes/>, 2018. [Online; accessed 10-April-2018].
- [43] Wikipedia. Total organic carbon. https://en.wikipedia.org/wiki/Total_organic_carbon, n.d. [Online; accessed 30-May-2018].
- [44] K. Wirth. X-ray fluorescence (xrf). https://serc.carleton.edu/research_education/geochemsheets/techniques/XRF.html, 2017. [Online; accessed 16-December-2017].
- [45] Özlem Bahadır Acıkara. Ion-exchange chromatography and its applications. In D. Martin, editor, *Column Chromatography*, chapter 2. InTech, Rijeka, 2013.

A Appendix

A.1 ICP-OES Calibration Curves

Calibration Curves for the metals on ICP-OES are as follows:

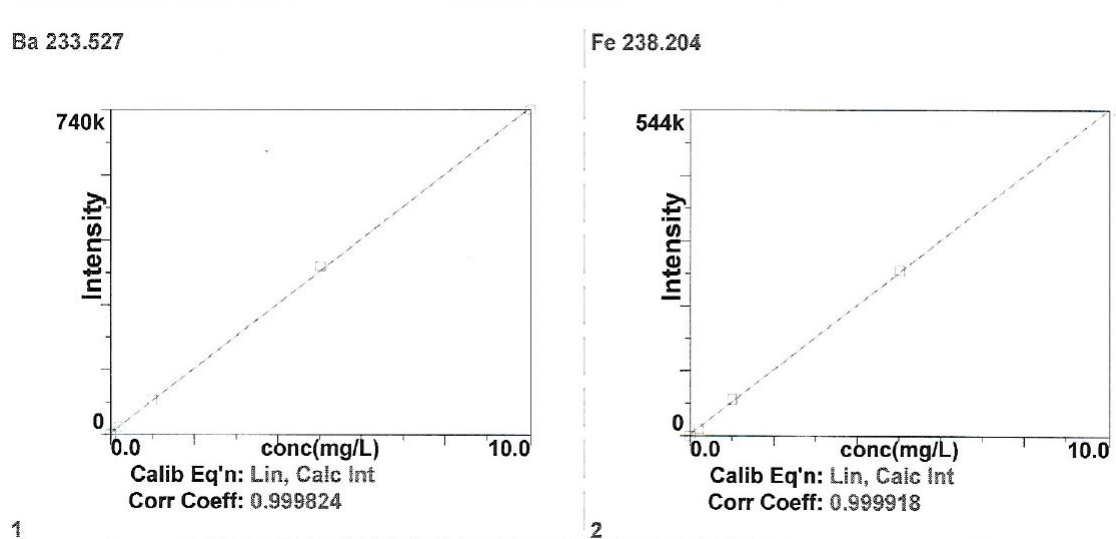


Figure A.1: Ba 233.527 and Fe 238.204 calibration curves, showing the correlation coefficient close to 1.

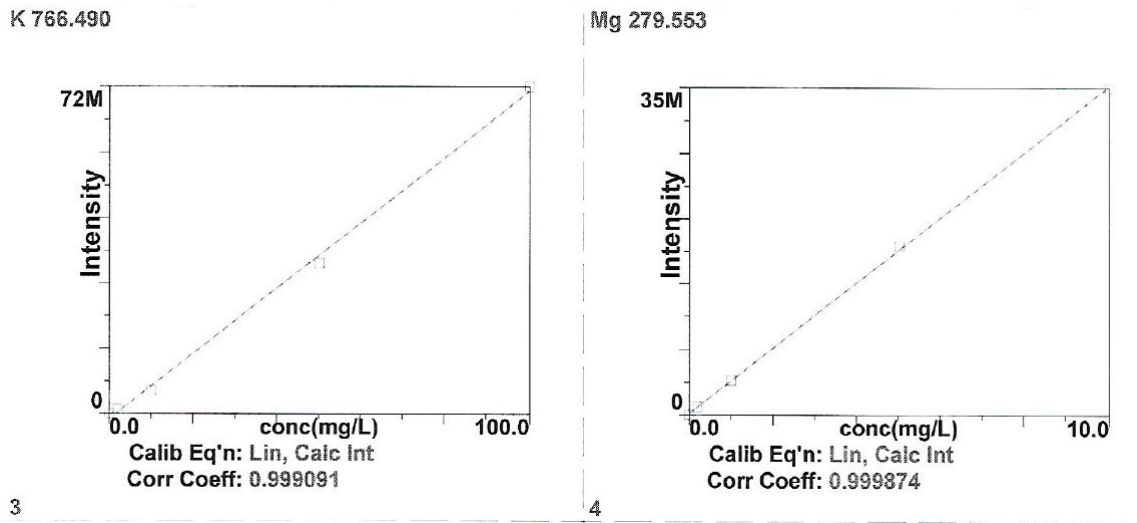


Figure A.2: K 766.490 and Mg 279.553 calibration curves, showing the correlation coefficient close to 1.

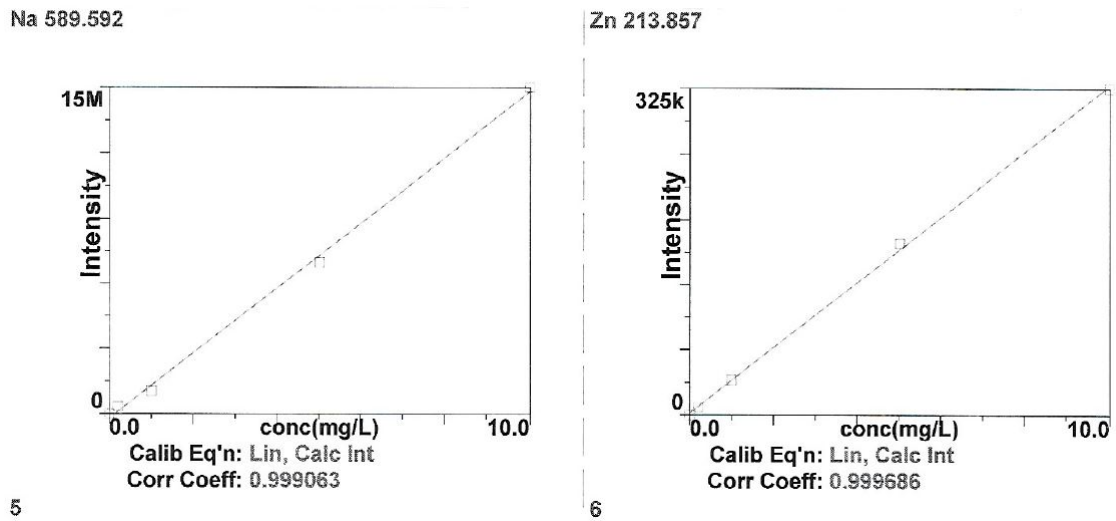


Figure A.3: Na 589.592 and Zn 213.857 calibration curves, showing the correlation coefficient close to 1.

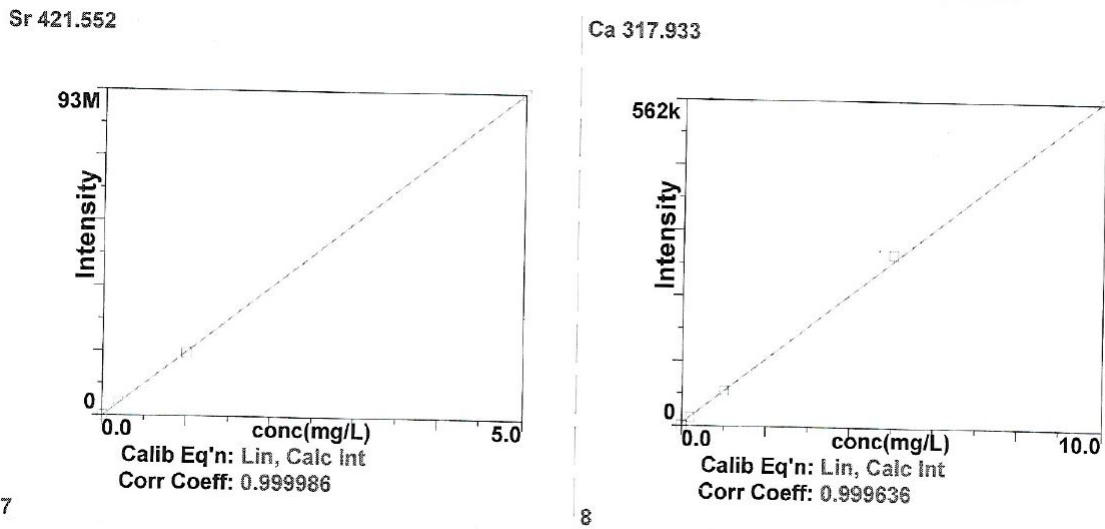


Figure A.4: Sr 421.552 and Ca 317.933 calibration curves, showing the correlation coefficient close to 1.

A.2 ICP-OES Spectrum

An example of ICP-OES spectrum for Na metal can be seen in Figure A.5.

Na 589.592

Rep: 3

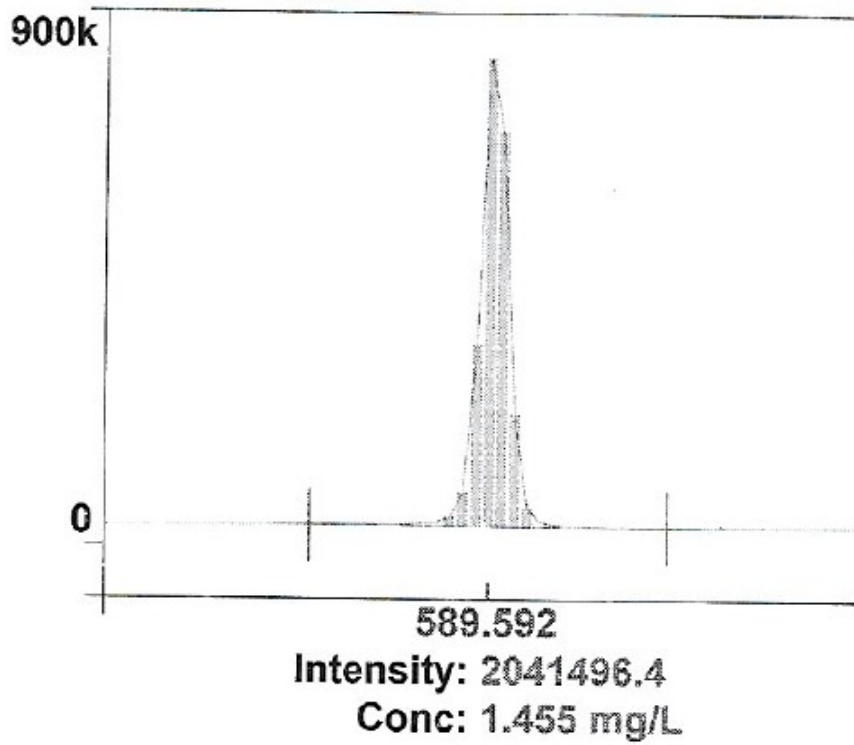


Figure A.5: Example of ICP-OES result provided for Na by Perkin Elmer Optima 8000 analyzer.

A.3 Ion Chromatography Calibration Curves

Calibration Curves for the major anions on Ion Chromatography are as follows:

1. Chloride calibration curve.

```
CALIBRATION OF COMPONENT chloride
Method: Anioner KEMI Erica PW.mtw
Equation: Q = 0.0105026 · A
RSD: 4.209 %
Correlation coefficient: 0.999200
```

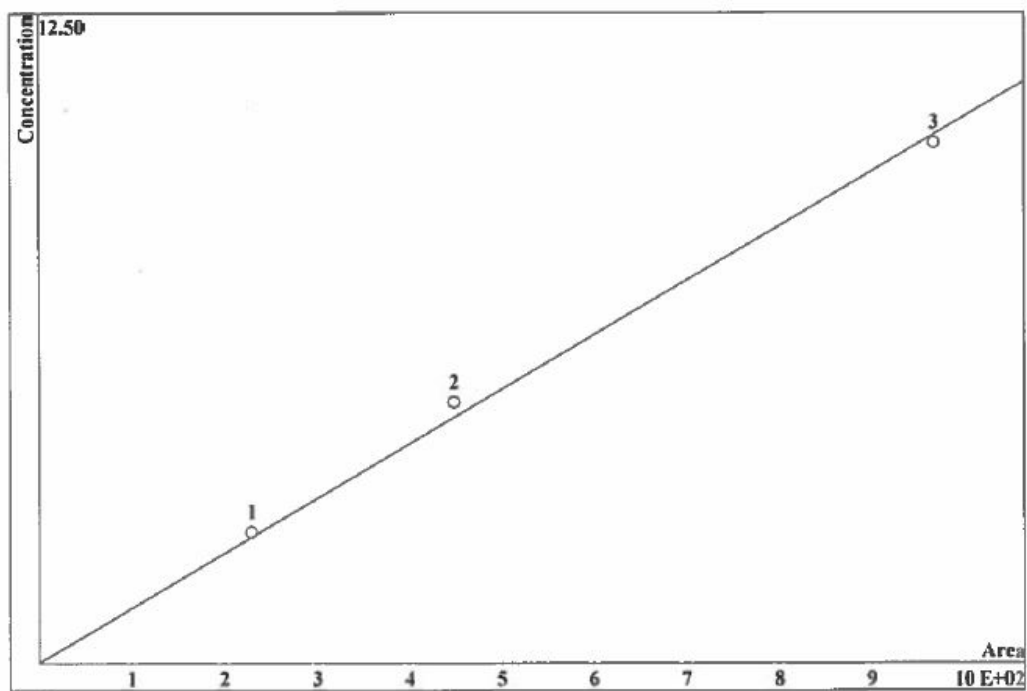


Figure A.6: Chloride ion calibration curve, showing the correlation coefficient close to 1.

2. Sulfate calibration curve.
3. Bromide calibration curve.

CALIBRATION OF COMPONENT sulphate

Method: Anioner KEMI Erica PW.mtw
Equation: $Q = 0.0165623 \cdot A$
RSD: 1.782 %
Correlation coefficient: 0.999886

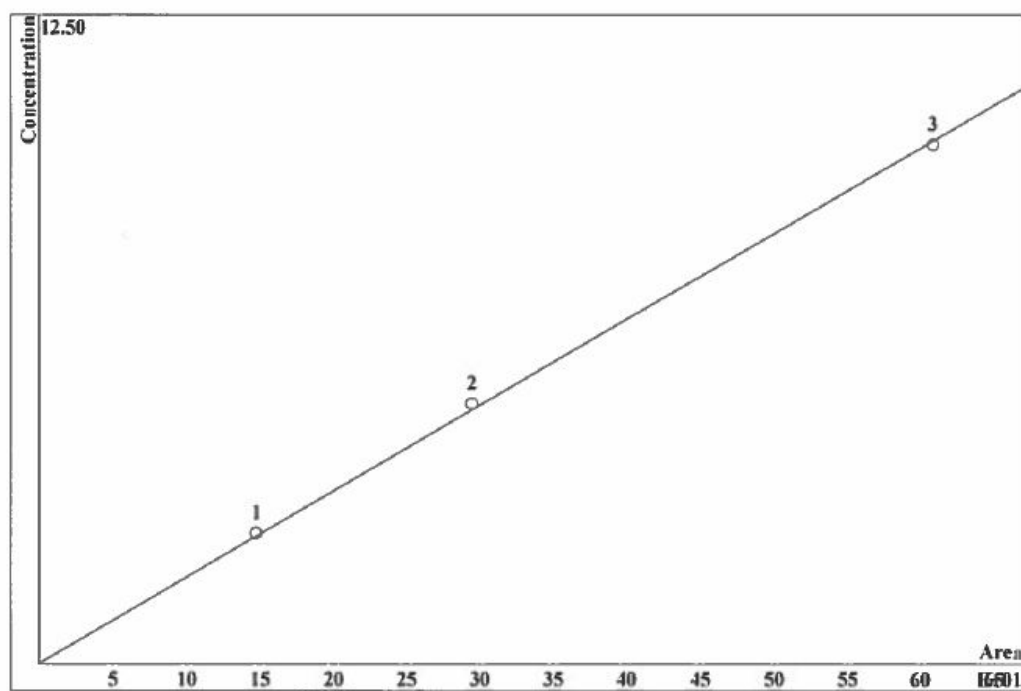


Figure A.7: Sulfate ion calibration curve, showing the correlation coefficient close to 1.

CALIBRATION OF COMPONENT bromide

Method: Anioner KEMI Erica PW.mtw
Equation: $Q = 0.0284214 \cdot A$
RSD: 2.357 %
Correlation coefficient: 0.999894

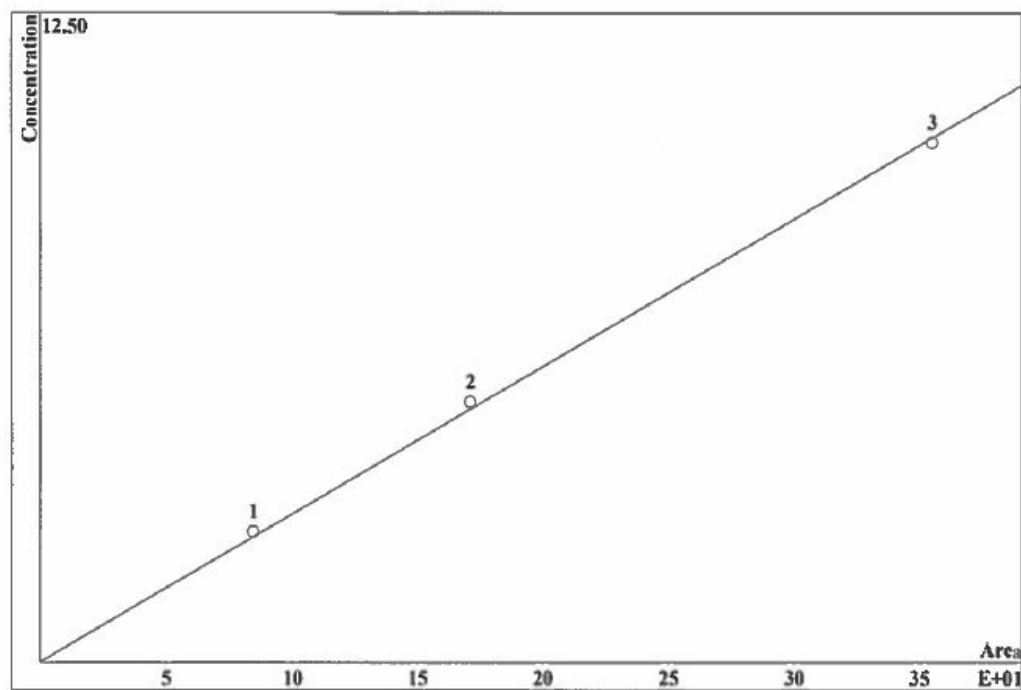


Figure A.8: Bromide ion calibration curve, showing the correlation coefficient close to 1.

A.4 Ion Chromatogram

An example of ion chromatogram can be seen in Figure A.9.

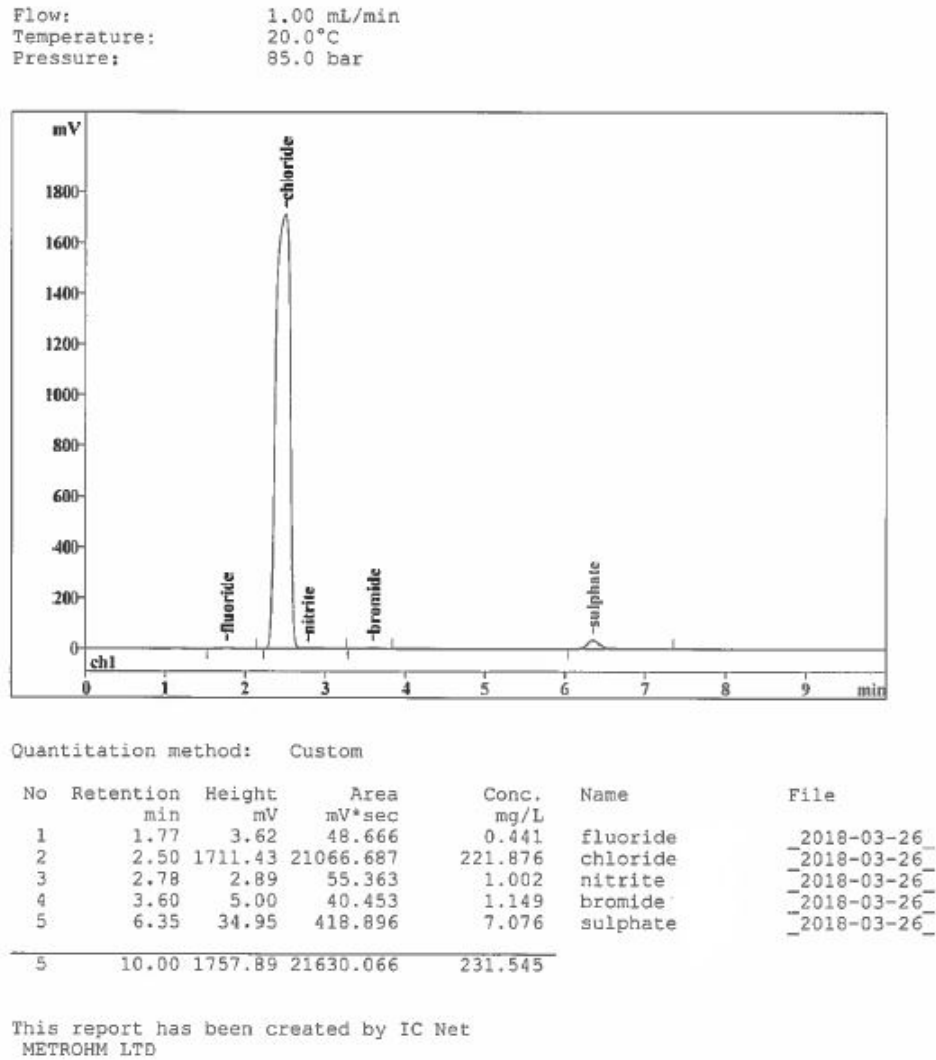


Figure A.9: Example of chromatogram result provided by Metrohm Ion Chromatography analyzer.